The Astrophysical Journal Letters, 995:L27 (19pp), 2025 December 10 https://doi.org/10.3847/2041-8213/ae2125

Pan-STARRS Follow-up of the Gravitational-wave Event S250818k and the Light Curve of SN2025ulz

J. H. Gillanders[1], M. E. Huber[2], M. Nicholl[3], S. J. Smartt[1,3], K. W. Smith[1,3], K. C. Chambers[2], D. R. Young[3], J. W. Tweddle[1], S. Srivastav[1], M. D. Fulton[3], F. Stoppa[1], G. S. H. Paek[2], A. Aamer[3], M. R. Alarcon[4,5], A. Andersson[1], A. Aryan[6], K. Auchettl[7,8], T.-W. Chen[6], T. de Boer[2], A. K. H. Kong[9], J. Licandro[4,5], T. Lowe[2], D. Magill[3], E. A. Magnier[2], P. Minguez[2], T. Moore[10], G. Pignata[11], A. Rest[10,12], M. Serra-Ricart[4,5,13], B. J. Shappee[2], I. A. Smith[14], M. A. Tucker[15,16,17], and R. Wainscoat[2]

[1] Astrophysics sub-Department, Department of Physics, University of Oxford, Keble Road, Oxford, OX1 3RH, UK; james.gillanders@physics.ox.ac.uk
[2] Institute for Astronomy, University of Hawai'i, 2680 Woodlawn Drive, Honolulu, HI 96822, USA
[3] Astrophysics Research Centre, School of Mathematics and Physics, Queen's University Belfast, BT7 1NN, UK
[4] Instituto de Astrofísica de Canarias (IAC), C/ Vía Láctea, s/n, E-38205, La Laguna, Spain
[5] Departamento de Astrofísica, Universidad de La Laguna (ULL), E-38206 La Laguna, Canarias, Spain
[6] Graduate Institute of Astronomy, National Central University, 300 Jhongda Road, 32001 Jhongli, Taiwan
[7] Department of Astronomy and Astrophysics, University of California, Santa Cruz, CA 95064, USA
[8] OzGrav, School of Physics, The University of Melbourne, VIC 3010, Australia
[9] Institute of Astronomy, National Tsing Hua University, Hsinchu 300044, Taiwan
[10] Space Telescope Science Institute, 3700 San Martin Drive, Baltimore, MD 21218, USA
[11] Instituto de Alta Investigación, Universidad de Tarapacá, Casilla 7D, Arica, Chile
[12] Department of Physics and Astronomy, Johns Hopkins University, Baltimore, MD 21218, USA
[13] Light Bridges, SL. Observatorio Astronómico del Teide, Carretera del Observatorio del Teide, s/n, Güímar, Santa Cruz de Tenerife, Spain
[14] Institute for Astronomy, University of Hawai'i, 34 Ohia Ku St., Pukalani, HI 96768-8288, USA
[15] Center for Cosmology and AstroParticle Physics, 191 W Woodruff Ave, Columbus, OH 43210, USA
[16] Department of Astronomy, The Ohio State University, 140 W 18th Ave, Columbus, OH 43210, USA
Received 2025 October 1; revised 2025 November 5; accepted 2025 November 16; published 2025 December 8

Abstract

Kilonovae are the scientifically rich—but observationally elusive—optical transient phenomena associated with compact binary mergers. Only a handful of events have been discovered to date, all through multiwavelength (gamma-ray) and multimessenger (gravitational-wave) signals. Given their scarcity, it is important to maximise the discovery possibility of new kilonova events. To this end, we present our follow-up observations of the gravitational-wave signal S250818k—a plausible binary neutron star merger at a distance of 237 ± 62 Mpc. Pan-STARRS tiled 286 and 318 deg^2 (32% and 34% of the 90% sky localisation region) within 3 and 7 days of the GW signal, respectively. ATLAS covered 65% of the sky map within 3 days, but with lower sensitivity. These observations uncovered 47 new transients; however, none were deemed to be linked to S250818k. We undertook an expansive follow-up campaign of AT2025ulz, the purported counterpart to S250818k. The *griz*-band light curve, combined with our redshift measurement ($z = 0.0849 \pm 0.0003$), all indicate that SN2025ulz is a type IIb supernova and thus not the counterpart to S250818k. We rule out the presence of an AT2017gfo-like kilonova within ≈27% of the distance posterior sampled by our Pan-STARRS pointings (≈9.1% across the total 90% 3D sky localisation). We demonstrate that early observations are optimal for probing the distance posterior of the 3D gravitational-wave sky map, and that SN2025ulz was a plausible kilonova candidate for $\lesssim$5 days, before ultimately being ruled out.

Unified Astronomy Thesaurus concepts: Supernovae (1668); Gravitational waves (678); Sky surveys (1464); Neutron stars (1108)

1. Introduction

The historic gravitational-wave (GW) event GW170817, resulting from a binary neutron star (BNS) merger (B. P. Abbott et al. 2017a), produced the short gamma-ray burst (GRB) 170817A (B. P. Abbott et al. 2017b) and the rapidly evolving UV–optical–IR transient AT2017gfo, the first confirmed kilonova (KN) event (B. P. Abbott et al. 2017c; I. Arcavi et al. 2017b; D. A. Coulter et al. 2017; V. M. Lipunov et al. 2017; M. Soares-Santos et al. 2017; N. R. Tanvir et al. 2017; S. Valenti et al. 2017). Further high-cadence spectrophotometric observations followed, which confirmed the uniqueness of the electromagnetic (EM) transient (R. Chornock et al. 2017; C. McCully et al. 2017; M. Nicholl et al. 2017; E. Pian et al. 2017; B. J. Shappee et al. 2017; S. J. Smartt et al. 2017). Extensive data acquisition and modeling followed (I. Andreoni et al. 2017; P. S. Cowperthwaite et al. 2017; M. R. Drout et al. 2017; P. A. Evans et al. 2017; M. M. Kasliwal et al. 2017; C. D. Kilpatrick et al. 2017; N. R. Tanvir et al. 2017; E. Troja et al. 2017; Y. Utsumi et al. 2017), which provided excellent matches to theory predictions, demonstrating that AT2017gfo was powered by the radioactive decay of neutron-rich *r*-process material (L.-X. Li & B. Paczyński 1998; B. D. Metzger et al. 2010; D. Kasen et al. 2013, 2017; M. Tanaka & K. Hotokezaka 2013; S. Rosswog et al. 2018).

Although other NS-bearing systems have since been detected by LIGO–Virgo–KAGRA (LVK), including the BNS merger GW190425 (B. P. Abbott et al. 2020) and the

[17] CCAPP Fellow.

NS–black hole (NSBH) mergers GW190814 (R. Abbott et al. 2020), GW200105, GW200115 (R. Abbott et al. 2021), GW230518, and GW230529 (A. G. Abac et al. 2024; The LIGO Scientific Collaboration et al. 2025b), GW170817 has remained the only GW source with a confirmed EM counterpart.

No KNe have been uncovered by widefield surveys (such as the Zwicky Transient Facility or ZTF and Pan-STARRS or PS; I. Andreoni et al. 2020; M. D. Fulton et al. 2025). J. C. Rastinejad et al. (2025) present analysis of eight proposed KNe (including AT2017gfo) associated with GRB signals. Of these, the three best-sampled events are the recent GRBs 160821B (G. P. Lamb et al. 2019), 211211A (J. C. Rastinejad et al. 2022; E. Troja et al. 2022), and 230307A (J. H. Gillanders et al. 2023; A. J. Levan et al. 2024; Y.-H. Yang et al. 2024). However, GRB-discovered KNe suffer from early-time contamination from the on-axis afterglow—an inevitable consequence of the fact we are only sensitive to on-axis events. GW signals are one of the best methods to ultimately enable uncontaminated early-time observations of KNe.

In this manuscript, we outline our follow-up observations of the GW event S250818k—possibly just the third astrophysically real BNS merger event—with PS and ATLAS. We also summarize our targeted observational campaign for SN2025ulz, which was proposed as a candidate optical counterpart (R. Stein et al. 2025). S250818k was discovered on MJD 60905.055625 (2025 August 18 01:20:06.030 UTC), and the alert was released at MJD 60905.055961 (The LIGO Scientific Collaboration et al. 2025a). This was initially classified as either a BNS merger (29% probability) or a terrestrial source (71% probability) by LVK, with an estimated distance of 263 ± 75 Mpc. A later improvement in the analysis, presented in the `bilby.fits` sky map, updated the distance estimate to 237 ± 62 Mpc, without changing the source classification probabilities.

Throughout, we adopt Planck ΛCDM cosmology with a Hubble constant, $H_0 = 67.4\,\mathrm{km\,s^{-1}\,Mpc^{-1}}$, $\Omega_M = 0.315$, and $\Omega_\Lambda = 0.685$ (Planck Collaboration et al. 2020). Also, all magnitudes are presented in the AB system (J. B. Oke & J. E. Gunn 1983).

2. S250818k

S250818k was discovered on MJD 60905.055625 and announced publicly on MJD 60905.055961 as a subthreshold GW event, with a false-alarm rate (FAR) of $2.1\,\mathrm{yr^{-1}}$ (The LIGO Scientific Collaboration et al. 2025a). As such, it did not pass our trigger criteria for immediate follow-up with either PS or ATLAS, due to its high probability of terrestrial origin ($p_{\rm terr} = 71\%$). However, additional investigation of the properties of the GW signal compared with the GW triggers from LVK's third observing run (O3; R. Abbott et al. 2023) show that, despite the apparent high likelihood of terrestrial origin, the signal properties broadly match those of previously reported high-significance candidate merger events.

Specifically, we apply the method of M. Nicholl & I. Andreoni (2025) to analyze the location of S250818k in the multi-dimensional parameter space of the FAR, $p_{\rm terr}$, luminosity distance (d_L), distance uncertainty (σ_{d_L}), and 90% localization area (A_{90}) multiplied by the number of active GW detectors ($n_{\rm det}$), as reported in low latency. The results are shown in Figure 1. S250818k lies in the typical distribution of the FAR versus $p_{\rm terr}$ for O3 triggers, though in a region dominated by spurious sources that were later retracted. Unsurprisingly, these parameters are correlated, with a high $p_{\rm terr}$ for events with a high FAR. However, S250818k does not have the highest $p_{\rm terr}$ for a candidate NS-bearing GW signal; this title belongs to the NSBH merger S200105ae, which, despite having $p_{\rm terr} = 0.97$ (and FAR $> 24\,\mathrm{yr^{-1}}$) in low latency, did survive in the offline analysis and was included in the third and fourth Gravitational Wave Transient Catalogs (GWTC-3 and GWTC-4) as a marginal event (R. Abbott et al. 2023; The LIGO Scientific Collaboration et al. 2025c). This event was also subject to intensive EM follow-up (S. Anand et al. 2021), though without an identified counterpart.

In all other parameters, S250818k sits in the locus of real events, away from the bulk of spurious ones. As noted by M. Nicholl & I. Andreoni (2025), the strongest discriminator between real and spurious GW detections arises from the σ_{d_L}/d_L versus d_L parameter space; here, we find that real events tend to lie in the lower right of the figure, whereas most of the spurious detections lie in the upper left region. S250818k also sits within the locus of NS-bearing events in terms of its localization area per detector (we also note that the LVK sky map for this event conformed to the expected smooth "banana" shape; see Figure 2). Based on these considerations, it would be unsurprising if S250818k was confirmed as a real astrophysical signal and, as such, we initiated our GW follow-up program with PS.

We do note one surprising parameter from the low-latency products. The chirp mass in S250818k was reported to lie (with 100% probability) in the 0.1–$0.87\,M_\odot$ bin. This parameter was not made public in low latency during O3, so we are unable to compare this to our control population of previous GW triggers. The constituent NS masses can be derived from the chirp mass ($\mathcal{M}$) via

$$\mathcal{M} = \frac{(m_1 \cdot m_2)^{3/5}}{(m_1 + m_2)^{1/5}}, \tag{1}$$

where m_1 and m_2 are the heavier and lighter NS masses, respectively. Expressing the mass of the lighter NS in terms of fractional mass of the heavier NS (i.e., $m_2 = \eta \cdot m_1$, where $0 < \eta \leqslant 1$) and rearranging gives

$$m_1 = \left(\frac{\eta + 1}{\eta^3}\right)^{1/5} \cdot \mathcal{M}. \tag{2}$$

For an equal-mass merger ($\eta = 1$), the upper edge of the chirp-mass bin ($\mathcal{M} = 0.87\,M_\odot$) corresponds to NS masses $m_1 \equiv m_2 = 1.0\,M_\odot$. For all forms of unequal mergers and for all chirp masses within the 0.1–$0.87\,M_\odot$ mass bin, $m_2 < 1\,M_\odot$. Thus, if this source is confirmed to be astrophysically real *and* the low-latency chirp mass is reliable, at least one of the components must have a mass $\leqslant 1\,M_\odot$.

3. Scanning the Sky Map of S250818k

3.1. Pan-STARRS

PS is a twin 1.8 m telescope system (Pan-STARRS1 and Pan-STARRS2 or PS1 and PS2), with both situated atop Haleakala mountain on the Hawaiian island of Maui (K. C. Chambers et al. 2016). PS1 has a 1.4 gigapixel camera, and the $0\farcs26$ pixels provide a focal plane with a diameter of $3\fdg0$ and a field-of-view (FOV) area of 7.06 deg^2. The PS2 telescope hosts a 1.5 gigapixel camera and supports a slightly

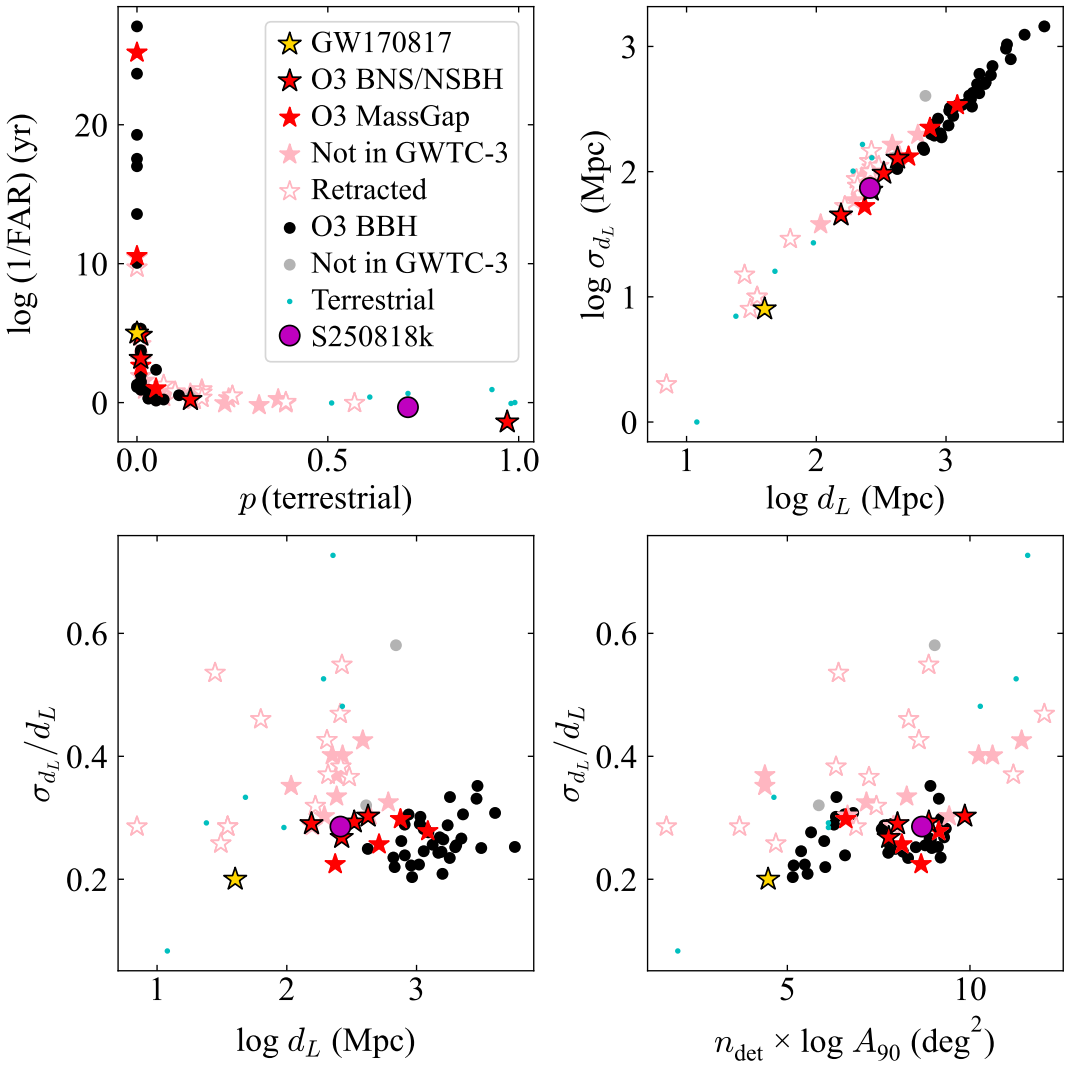

Figure 1. Comparison of the GW signal properties of S250818k to those from the LVK GWTC-3 catalog (R. Abbott et al. 2023), following M. Nicholl & I. Andreoni (2025).

larger FOV. Each telescope is equipped with the same filter system, denoted as $grizy_{ps}$ (as described by J. L. Tonry et al. 2012). Images from both PS telescopes are processed with the Image Processing Pipeline (IPP; E. A. Magnier et al. 2020a; C. Z. Waters et al. 2020).

The individual exposure frames (called warps) are astrometrically and photometrically calibrated (E. A. Magnier et al. 2020b), and overlapping exposures are coadded together with median clipping applied (to produce stacks). The PS1 3π reference sky images are subtracted from these frames (C. Z. Waters et al. 2020), and photometry is carried out on the resulting difference image (E. A. Magnier et al. 2020c). These individual detections are ingested into the PS Transient Server database and assimilated into distinct objects with a time-variable history. A series of quality filters are applied using the IPP image attributes, and known asteroids and variable stars are removed. The objects remaining are crossmatched with all cataloged galaxies, active galactic nuclei (AGNs), cataclysmic variables (CVs), and historical transients (K. W. Smith et al. 2020), and simultaneously a machine learning algorithm is applied to image pixel stamps at each transient position (D. E. Wright et al. 2015; K. W. Smith et al. 2020). This reduces the bogus detections to a manageable number for human scanning. For details of the filtering and our human scanning process, specifically in the context of GW follow-up and faint transient identification, the reader is referred to S. J. Smartt et al. (2024) and M. D. Fulton et al. (2025).

We began observing the LVK `bilby.fits` sky map (The LIGO Scientific Collaboration et al. 2025a) beginning on MJD 60907.298193—2.2426 days postburst (the night of 2025 August 20; Hawaii Standard Time). Our observations tiled the northern banana on three nights—2025 August 20, 21, and 22—with a series of dithered 45 and 120 s exposures taken, reaching total exposure times per skycell of 90–3975 s (median exposure time of 360 s) in the $i_{\rm ps}$ band. These images were combined into a single stacked image for each PS skycell (K. C. Chambers et al. 2016), and the standard processing as described above was immediately carried out. Typical 3.5σ limiting magnitudes of $m_{i_{\rm PS}} \simeq 19-23$ were achieved on these nightly stacks across the three nights, with the large range being due to varying sky conditions. We covered 286 and 318 deg^2 (32% and 34%) of the `bilby.fits` 90% sky localization region with PS within 3 and 7 days postburst, respectively. We summarize our discoveries in Section 4. Our PS tiling of the S250818k sky map is visually illustrated in Figure 2.

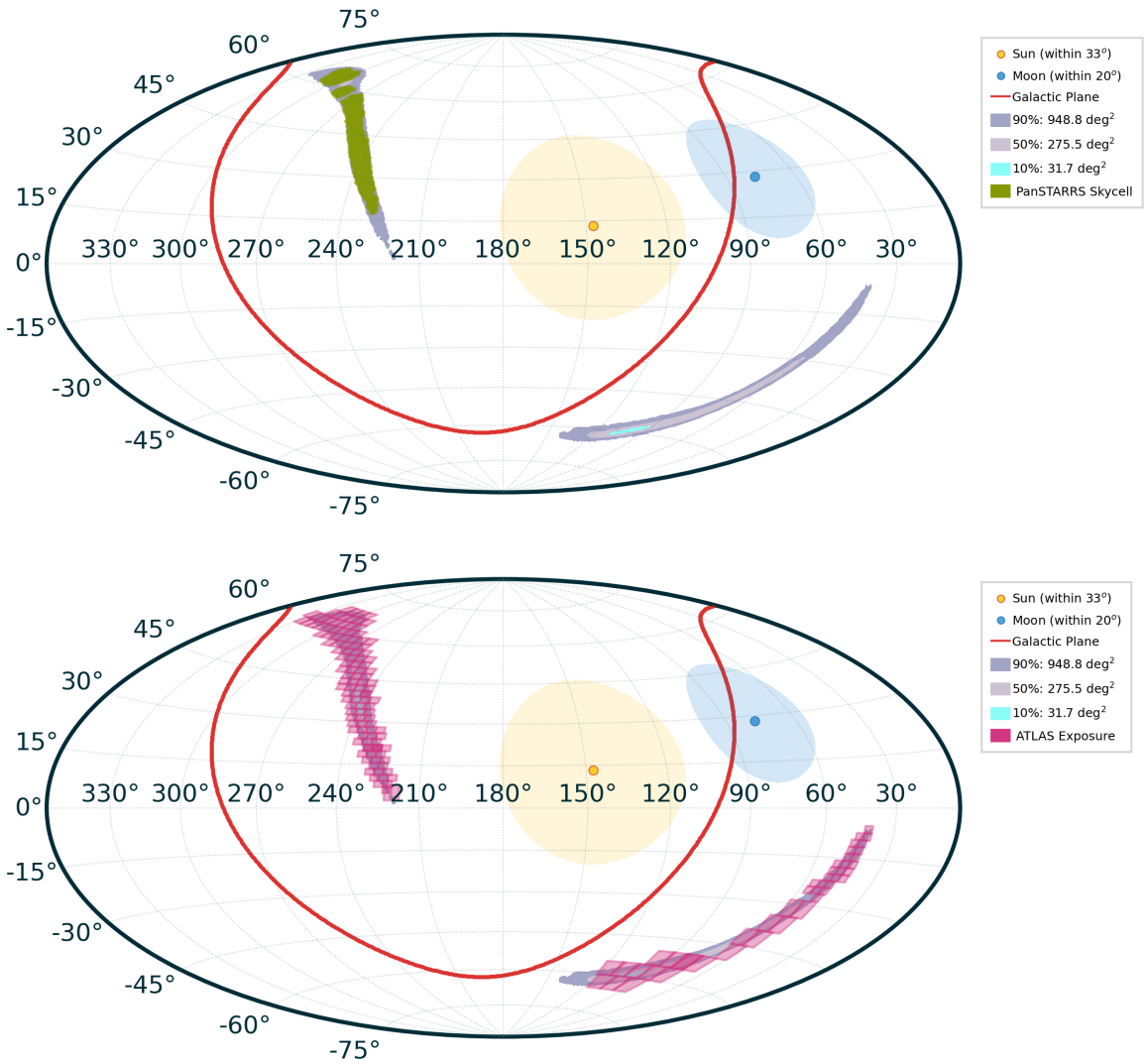

Figure 2. Top: the `bilby.fits` sky map from The LIGO Scientific Collaboration et al. (2025a), with our targeted PS tiling observations performed within 7 days postburst overlaid. Bottom: the same as above but with the ATLAS observation footprints within 7 days postburst overlaid.

3.2. ATLAS

The ATLAS system consists of five units, situated at Haleakala and Mauna Loa (Hawaii), El Sauce (Chile), Sutherland (South Africa), and Tenerife (Canary Islands) (J. L. Tonry et al. 2018b; J. Licandro et al. 2023). Together, they tile the entire visible sky every ∼24 hr (weather-dependent). The telescopes survey the sky in cyan (c) and orange (o), and the Tenerife unit uses a "wide" passband (w; CMOS response together with a UV/IR-cut filter—a similar effective wavelength to the combined Sloan $g' + r'$ bands). Typically, a pattern of 4 × 30 s dithered exposures is acquired each night (roughly spaced logarithmically within a 1 hr period). Our data processing pipeline follows standard practices; the images are photometrically and astrometrically calibrated using RefCat2 (J. L. Tonry et al. 2018a), before template subtraction is performed. As described by K. W. Smith et al. (2020), quality cuts are applied, cataloged objects are crossmatched, and machine learning algorithms are applied to the data to reject spurious detections and identify extragalactic transients (J. G. Weston et al. 2024; H. F. Stevance et al. 2025).

Similar to PS, we have a targeted GW follow-up program in place to rapidly tile the GW sky maps of candidate optical counterparts to GW signals (e.g., S. J. Smartt et al. 2024). Given the subthreshold nature of the reported GW signal S250818k, we did not initiate targeted follow-up searches. However, the ATLAS survey, during its routine sky survey mode, canvassed a substantial fraction of the `bilby.fits` sky map within the first few nights postburst. We note that during this period, ATLAS was undergoing a trial of extended exposures; as such, each ATLAS observation was composed of 4 × 110 s exposures, resulting in deeper stacked target images compared with the "default" observing strategy (440 versus 120 s).

The ATLAS coverage within 7 days postburst is illustrated in Figure 2. We sampled 219, 604, and 831 deg^2 (25%, 65%, and 81%) of the `bilby.fits` 90% sky localization region with ATLAS within 1, 3, and 7 days postburst, respectively. Each ATLAS pointing reached typical 5σ limiting magnitudes of $m_o \simeq 18.8$–20.4 (110 s) and $m_w \simeq 18.0$–20.6 (30 s). Searching these data did not return any convincing candidate counterparts to S250818k within the first 3 days after the GW signal.

4. Candidate Counterparts

From our PS scanning of the northern portion of the `bilby.fits` sky map on August 20, 21, and 22, we uncover 75 real extragalactic transient sources that lie within the 90% contour of the northern "banana." We found a fairly similar number of sources in our difference images that were faint and spatially coincident with the nucleus of a host galaxy or coincident with a nonextended source that was either stellar or a compact galaxy. We visually inspected all and found no evidence of significant light-curve changes (defined by $\Delta M \geqslant 0.2$ mag day^{-1} at more than 3σ significance) that would imply a measurement of evolving luminosity. We deemed these to be likely due to AGN variability or subtraction artifacts and thus did not consider them further. Our rejection of these is supported by the fact that $\lesssim$10% of short GRBs[18] occur within a host angular offset of 1″ (B. O'Connor et al. 2022). Of the 75 real extragalactic transient sources that are not obviously due to AGN variability, 28 had recorded activity prior to the GW burst and thus are unrelated to S250818k. The remaining 47 transients were reported to the IAU Transient Name Server (TNS);[19] for these, we perform some additional investigation, to determine their nature and the likelihood of them being the optical counterpart associated with S250818k. We searched for transients spatially associated with a host galaxy with a photometric[20] or spectroscopic redshift within the 2σ limit from the LVK `bilby.fits` sky map ($0.025 < z < 0.08$) that had no history of flux before S250818k in our PS and ATLAS survey data, or in the ZTF public stream (through the Lasair broker; R. D. Williams et al. 2024), or registered on the TNS, and absolute magnitudes that place them in the KN regime ($M \gtrsim -17$; B. D. Metzger et al. 2010; M. Bulla 2019; M. Nicholl et al. 2021). These criteria reduced the list of viable candidates to seven (excluding SN2025ulz; for information on SN2025ulz, see Section 5). The full list of new transient sources discovered is listed in Table 1, and we discuss our seven viable candidates below.

We draw attention to the limitations in our selection of the seven candidates. It is possible that KNe: (i) may be brighter than $M \sim -17$ (particularly if there is a long-lived neutron star; Y.-W. Yu et al. 2013; B. D. Metzger & A. L. Piro 2014); (ii) are nuclear; and/or (iii) lie in galaxies that have a redshift within the 3σ distance limit (rather than our 2σ cut). While we considered these unlikely, we still list the sources we have discounted as counterparts in Table 1. This table does not include the ∼70 low-significance sources that are spatially coincident with the centers of their hosts and show no obvious signature of being a source of interest. If a GW counterpart lies within this sample, we would be confusion-limited, and further data (e.g., high-energy/radio emission or a strong IR excess) would be required to distinguish the counterpart from the background of confounding sources.

4.1. Most Viable Candidates

AT2025uso/PS25grz. We first detected AT2025uso on MJD 60907.3, the first night of our targeted follow-up campaign, at $m_i = 20.47 \pm 0.18$ (S. J. Smartt et al. 2025), coincident with a host galaxy with a spectroscopic redshift within the LVK range ($z_{\rm spec} = 0.025$; DESI Collaboration et al. 2025). Although a promising candidate ($M_i \simeq -15$), further follow-up across the next two nights showed little light-curve evolution. Furthermore, ATLAS detected AT2025uso on MJD 60909.9 ∼1 magnitude brighter in w band and tracked a rise to peak at $m_o \sim 18$ over the following 20 days. Finally, the updated `bilby.fits` sky map resulted in AT2025uso lying outside the 90% localization region. Thus, we discount AT2025uso being related to S250818k.

AT2025usy/PS25gsa. We detected AT2025usy on the first night of targeted follow-up observations (2025 August 20; MJD 60907.4), as a new transient with $m_i = 20.95 \pm 0.27$ (S. J. Smartt et al. 2025), coincident with a galaxy with a recorded photometric redshift $z_{\rm phot} = 0.090 \pm 0.012$ (D. Schlegel et al. 2021), which would place it at $M_i \simeq -17$. The combination of the redshift of the host galaxy lying beyond the 2σ LVK limit, the bright absolute magnitude, and the light curve remaining flat (i.e., within the errors—there is no evidence for a change in magnitude) across the subsequent two nights of observation (out to MJD 60909.4) led to us disfavoring AT2025usy as a plausible candidate.

AT2025utr/PS25gsh. AT2025utr was discovered on MJD 60907.4 with $m_i = 19.84 \pm 0.13$ (S. J. Smartt et al. 2025), coincident with a galaxy with $z_{\rm phot} = 0.043 \pm 0.011$ (D. Schlegel et al. 2021). While a promising candidate (albeit on the brighter end), further observations up to MJD 60909.4 revealed a flat (within the errors) light-curve evolution. We scheduled further observations with PS (300 s i-band observation on MJD 60924.3) that confirmed the flat (or slightly rising) light-curve evolution inferred from the earlier observations ($m_i = 19.67 \pm 0.03$). Finally, ATLAS detected AT2025utr on MJD 60906.3 and observed its light curve rise in w and o across the next 15 days. The light curve resembles that of a supernova (i.e., its evolution follows the typical supernova ∼2–3 week rise to peak), and thus we rule out AT2025utr as a KN candidate counterpart to S250818k.

AT2025utx/PS25gsm. AT2025utx was discovered on MJD 60907.4 at $m_i = 20.21 \pm 0.26$. It is coincident with a galaxy with $z_{\rm spec} = 0.080$ (DESI Collaboration et al. 2025), which places it right at the upper 2σ bound for the LVK `bilby.fits` sky map localization (The LIGO Scientific Collaboration et al. 2025a). At this redshift, AT2025utx possessed an absolute magnitude $M_i = -17.6$, which is likely too bright for a KN, and further observations with PS (300 s i-band observation on MJD 60924.3) confirmed the flat light-curve evolution inferred from the earlier observations ($m_i = 20.12 \pm 0.11$). The flat light curve and bright magnitude compared to what we might expect for KNe rule out AT2025utx as a suitable candidate counterpart.

AT2025uuf/PS25gsv. AT2025uuf was detected on MJD 60907.4 at $m_i = 20.99 \pm 0.29$ (S. J. Smartt et al. 2025). It is coincident with a galaxy with $z_{\rm phot} = 0.061$ (M. Bilicki et al. 2014), within the LVK distance range. The inferred absolute magnitude of $M_i \sim -16$ would put it in the KN regime, but subsequent observations across the next two nights (up to MJD 60909.6) revealed no sign of decline and a flat light-curve evolution. Further observations with PS (300 s i-band observation on MJD 60924.3) confirmed the flat (or slightly rising) light-curve evolution inferred from the earlier observations ($m_i = 20.58 \pm 0.11$), and thus we suggest AT2025uuf is likely a supernova and not associated with S250818k.

[18] Short GRBs are produced by compact binary mergers (C. Kouveliotou et al. 1993; E. Berger et al. 2013; N. R. Tanvir et al. 2013) and are thus a useful proxy for any candidate BNS merger counterpart.

[19] www.wis-tns.org

[20] Photometric redshift estimates can be uncertain at these low redshifts, and so we only utilize these for the cases where spectroscopic redshift information is not available.

AT2025uuw/PS25gtm. We detected AT2025uuw on MJD 60907.4 with an initial AB magnitude $m_i = 20.44 \pm 0.20$ (S. J. Smartt et al. 2025), coincident with a galaxy with a photometric redshift $z_{\rm phot} = 0.034 \pm 0.006$ (D. Schlegel et al. 2021). Follow-up observations on MJD 60909.3 revealed a rising source, and further observations with PS (300 s *i*-band observation on MJD 60924.2) showed substantial brightening from the previous epochs of observation, with the *i*-band magnitude rising by more than 2 magnitudes ($m_i = 18.10 \pm 0.02$). ATLAS detected AT2025uuw on MJD 60911.0 in the *w* band and tracked its brightening in *w* and *o*. Finally, AT2025uuw was classified as an SN Ia at $z = 0.03$ (C. Fremling et al. 2025).

AT2025uxs/PS25guo. We discovered AT2025uxs on MJD 60909.3, the third night of our targeted follow-up observations (S. J. Smartt et al. 2025). It was detected with $m_i = 20.05 \pm 0.08$ and associated with a galaxy with $z_{\rm spec} = 0.063$ (DESI Collaboration et al. 2025), giving AT2025uxs an absolute AB mag $M_i = -17.2$. Further observations with PS (300 s *i*-band observation on MJD 60924.2) showed substantial brightening ($m_i = 18.48 \pm 0.02$), and ATLAS data showed a rising light curve in *w* and *o* for the subsequent 15 days. The light curve again resembles a supernova, and thus we conclude that AT2025uxs is not a KN-like source associated with S250818k.

In summary, from our targeted sky map tiling with PS, and routine ATLAS observations, we uncover no convincing optical KN-like counterpart candidates to the GW event S250818k. However, we note that we were only able to cover the northern banana with PS, and our follow-up campaign commenced ≈2.2 days postburst, and so we may not have been sensitive to an optical counterpart, were it faint and rapidly evolving (a point we consider further in Section 6).

4.2. Alternative Counterpart Scenario

B. D. Metzger et al. (2024) and Y.-X. Chen & B. D. Metzger (2025) present a scenario to explain the potential for subsolar-mass NS (ssNS) mergers, possibly detectable via GWs by LVK. In this scenario, ssNSs are formed in the gaseous accretion disk surrounding a young collapsar event. These ssNSs then potentially undergo multiple mergers on a rapid timescale (minutes–hours; at most ⩽days), with each merger possibly producing a detectable GW signal. Interestingly, the optical counterparts to these systems will not appear as a "typical" KN signal; any signal powered from *r*-process radioactive decay will be dwarfed by the radiation emitted from the collapsar. Thus, it may be the case that the optical signal one should search for as the counterpart to ssNS merger GW signals is that of a collapsar (possibly with some boosted emission from the KN(e) within the system).

We performed a search for a coincident collapsar signal in our ATLAS and PS (and all publicly available) data. Specifically, we scanned all TNS-registered events for SN-like transients that were located within the `bilby.fits` sky map (including those discussed above), associated with a galaxy within the 2σ distance limit of the GW signal, and with a plausible explosion epoch $\lesssim$3 days post-GW-signal. From this search, we do not uncover any convincing counterpart signal. This is perhaps not so surprising, given that one of the predictions of the scenario presented by B. D. Metzger et al. (2024) and Y.-X. Chen & B. D. Metzger (2025) is that a sequence of merger events may occur in quick succession, producing multiple, independent, GW signals. No subsequent related GW events were reported prior to, or following, S250818k.

We note that future optical follow-up campaigns for GW triggers (especially those for ssNS mergers) should consider this merger scenario, as it provides an alternative distinct optical signature for which one can search. In this scenario, we would not be searching for rapidly fading faint optical transients (on timescales of ∼days) but rather rising SN-like sources that would need to be followed and quantified for many weeks.

5. SN2025ulz

5.1. Initial Discovery and Observations

AT2025ulz was discovered by ZTF (E. C. Bellm et al. 2019) during its follow-up observations tiling the localization region of S250818k, with AB magnitudes $m_g = 20.99 \pm 0.13$ and $m_r = 21.29 \pm 0.13$ (R. Stein et al. 2025). The ZTF coverage of the sky map began quickly, just 2.7 hr after the GW trigger (R. Stein et al. 2025), and follow-up observations revealed that AT2025ulz was fading quickly and changing color (M. Busmann et al. 2025; X. J. Hall et al. 2025). While the position of AT2025ulz was covered in our PS tiling of the map of S250818k, we also triggered targeted follow-up observations of AT2025ulz with PS in $grizy_{ps}$ with longer exposures, due to the report of $m_r = 21.8$ mag from X. J. Hall et al. (2025) and its fading nature.

We commenced observing on the night of 2025 August 20 (MJD 60907.3), approximately 2.2 days postburst (J. H. Gillanders et al. 2025). We continued nightly multicolor monitoring of AT2025ulz alongside our follow-up program tiling the S250818k sky map (as outlined in Section 3.1). We began with a nightly cadence until ≃8 days postburst, where we then relaxed to a 2–4 day cadence. We dropped the *zy* bands after observations on MJD 60908.2 returned only upper limits. S. Banerjee et al. (2025b) obtained a spectrum of AT2025ulz on MJD 60911.0 and classified the transient as an SN IIb. Despite this classification, we continued our monitoring of SN2025ulz (now classified as an SN on the TNS), as it presented a good opportunity to sample and characterize a source that, at least initially, seemed a promising candidate counterpart to S250818k.

We also undertook targeted observations of SN2025ulz with the 40 cm Super Light Telescope (SLT) and Lulin One-meter Telescope (LOT) at the Lulin observatory, in the Sloan Digital Sky Survey (SDSS) *ugri* filters, as part of the Kinder collaboration (T.-W. Chen et al. 2025). These images were calibrated using a custom-built pipeline (H.-Y. Miao 2022), and photometry was measured using the AUTOPHOT pipeline (S. J. Brennan & M. Fraser 2022). A full summary of our follow-up photometric observations is presented in Table 2 and illustrated in Figure 3.

At the PS sky location of SN2025ulz (R.A. = $237.^{\circ}97584$, decl. = $+30.^{\circ}90241$), the STScI PS1 3π stamp server reference frames are shallower than our stacked target images (H. A. Flewelling et al. 2020). The subtraction of a reference template shallower than the science image can lead to substantial systematic errors in measuring reliable photometry for the transient. Specifically, we find that use of the PS1 3π *i*-band reference images results in systematic offsets from the true photometry of order $\lesssim$0.8 mag. Since the release of the PS1 DR2 images at STScI, both PS1 and PS2 have continued observing, and in certain regions of the sky we can construct significantly deeper reference images from this proprietary data. Our new stacked reference frames sum to total exposure

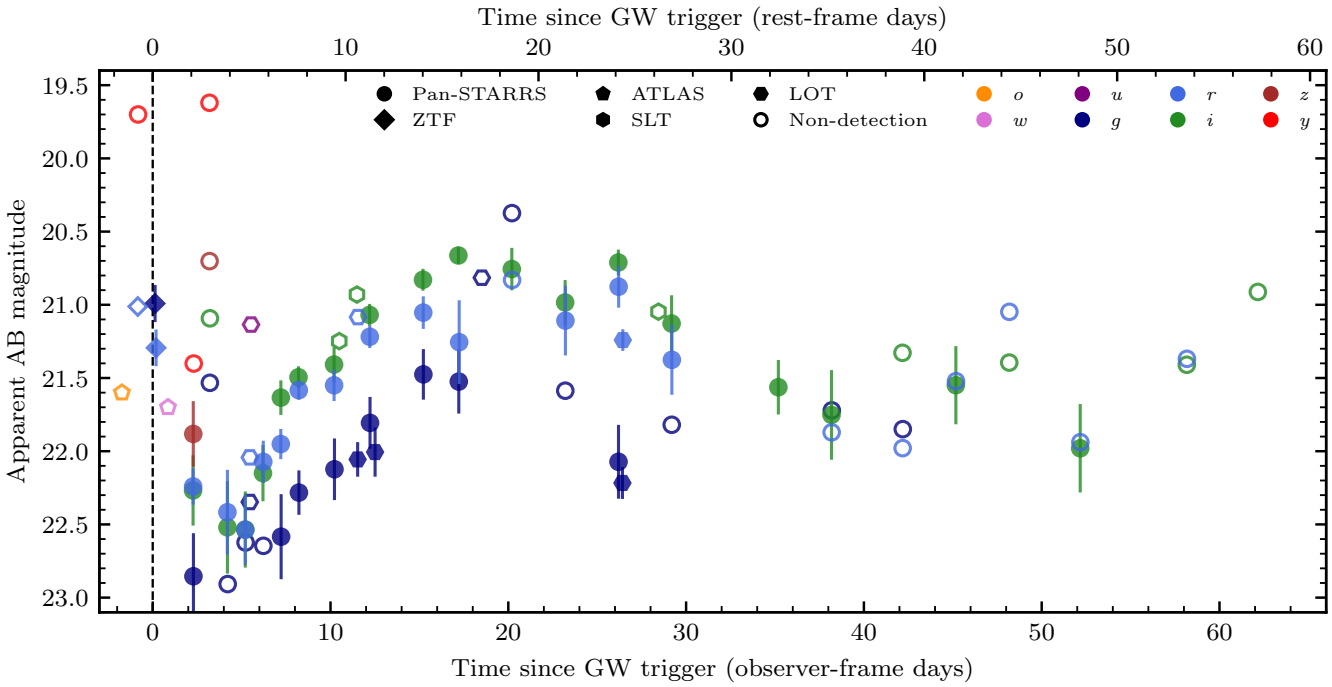

Figure 3. Light curve of SN2025ulz. We include the discovery *gr*-band data from ZTF (R. Stein et al. 2025) in addition to our multicolor PS, ATLAS, SLT, and LOT data. The hollow symbols correspond to 3σ upper limits.

times for each of $izy_{\rm ps}$ of $t_i = 4445$, $t_z = 6720$ and $t_y = 2760$ s, respectively.[21] Using these as reference templates allows us to extract accurate photometry for SN2025ulz, as well as ensure reliable host galaxy subtraction—a vital step, given the proximity of the transient to the host galaxy nucleus. To enable robust analysis of SN2025ulz by other groups, we provide public access to these improved reference frames (see the Data Availability section).

5.2. Historical Activity Search in PS and ATLAS

To check for any prior transient or variable activity of this source, we searched the location of SN2025ulz in our PS data. We uncover two recent nondetections ($m_i > 21.0$ at 9.7 days preburst and $m_y > 19.7$ at 0.82 days preburst; both 3σ upper limits) at the location of SN2025ulz (first reported by M. Nicholl et al. 2025). These data, in particular the *y*-band upper limit, place useful constraints on the presence of a bright transient at the location of SN2025ulz immediately prior to the GW merger.

Despite not being as sensitive as the PS survey, ATLAS can still provide useful constraints on premerger activity, especially given its high-cadence sky coverage. We forced flux measurements at the sky position of SN2025ulz in all ATLAS difference images for a period of 50 days before the discovery of S250818k (using the ATLAS Forced Photometry Server; L. Shingles et al. 2021). This includes 28 separate nights of observations by the ATLAS telescopes during that time. The individual 30 and 110 s (see Section 3.2) frame fluxes and errors were combined into one nightly measurement. We can confirm that no previous source existed at this position within the ATLAS data down to a 3σ limiting magnitude, $m_o \sim 19.8$–21.6. The most recent pre-GW-trigger ATLAS observation of the location of SN2025ulz was performed at MJD 60903.322 (1.73 days preburst), and from these pointings, we were able to obtain a 3σ limiting magnitude of $m_o > 21.6$ (S. Srivastav et al. 2025). ATLAS also observed the field on MJD 60905.916 (0.86 days postburst), yielding a 3σ upper limit of $m_w > 21.7$ at the position of SN2025ulz.

5.3. Redshift Estimation

SN2025ulz is offset from the center of its host galaxy WISEA J155154.15+305409.2 by $0\farcs88$. At the time of discovery of SN2025ulz by ZTF, only a photometric redshift, $z_{\rm phot} = 0.091 \pm 0.016$ (D. Schlegel et al. 2021), was available. We performed an observation of the host galaxy with the SuperNova Integral Field Spectrograph (SNIFS) instrument (B. Lantz et al. 2004) on the University of Hawaii 2.2 m telescope at Maunakea, beginning on 2025 September 2, with an exposure time of 2700 s. SNIFS has two channels, split by a dichroic mirror, spanning 3400–5100 Å and 5100–10000 Å, with average spectral resolutions of 5 Å and 7 Å for the Blue and Red channels, respectively. The data were processed with the quick nightly reduction pipeline described by M. A. Tucker et al. (2022).

In this spectrum (Figure 4), we identify prominent emission features centered at 7119 Å, 7142 Å, 7286 Å, and 7302 Å, which correspond to galaxy emission lines of Hα, [N II] λ6583.46, and [S II] $\lambda\lambda$6716.44& 6730.81, respectively, at a redshift $z = 0.0849 \pm 0.0003$. This measurement for the host redshift is in agreement with other measurements reported by V. Karambelkar et al. (2025) and S. Banerjee et al. (2025b).

For our chosen cosmological parameters (see Section 1), the redshift of SN2025ulz corresponds to a luminosity distance $D_{\rm L} \approx 401$ Mpc. This lies just within the reported 2σ limit for the distance in the `bilby.fits` sky map in the direction of SN2025ulz, which is $D_{\rm L} = 266 \pm 70$ Mpc.

5.4. Observed Properties of SN2025ulz

The first peak of SN2025ulz is short-lived, with its maximum occurring before our first PS observation. The discovery *gr*-band

[21] We do not possess many historical *gr*-band images and so rely on the original DR2 templates, with total exposure times of $t_g = 817$ and $t_r = 960$ s.

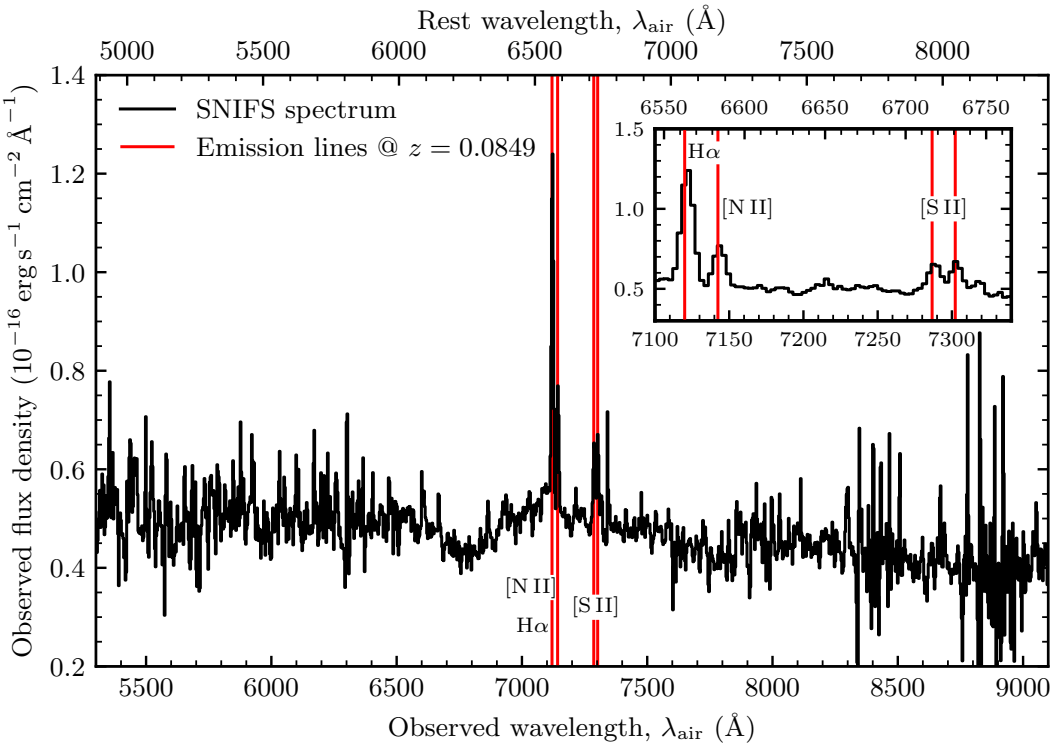

Figure 4. SNIFS spectrum of the host galaxy of SN2025ulz. We mark the location of prominent Hα, [N II] λ6583.46, and [S II] λλ6716.44 & 6730.81 emission, which allows us to measure a host galaxy redshift $z = 0.0849 \pm 0.0003$.

magnitudes from ZTF (R. Stein et al. 2025), acquired just 0.13 and 0.19 days after the GW trigger, at $m_g = 20.99 \pm 0.13$ and $m_r = 21.29 \pm 0.13$, respectively (R. Stein 2025), are the brightest reported in General Coordinates Network (GCN) Circulars and on the TNS from this early phase, and so we assume them to be at (or close to) peak. We measured SN2025ulz to rapidly fade from this peak to $m_g = 22.85 \pm 0.29$ and $m_r = 22.24 \pm 0.12$ in our first PS *gr*-band observations, acquired at 2.29 and 2.27 days postmerger, respectively, corresponding to decline rates of 0.86 mag day^{-1} (*g*) and 0.45 mag day^{-1} (*r*). For comparison, AT2017gfo had a *g*-band (*r*-band) fade rate of 1.55 mag day^{-1} (1.15 mag day^{-1}) from 1.4 to 2.4 days postexplosion (see Section 5.6). The color of SN2025ulz evolved rapid in this early phase, too, from $g - r \approx -0.3$ at discovery to $g - r \approx +0.6$ in the PS observations at 2.3 days.

The Milky Way extinction toward the line of sight of SN2025ulz is $E(B - V) = 0.0244$, and in the PS1 filters (assuming $R_V = 3.1$) this corresponds to $A_g = 0.090$, $A_r = 0.065$, $A_i = 0.048$, $A_z = 0.038$, $A_y = 0.031$, and $A_w = 0.067$ AB mag (E. F. Schlafly & D. P. Finkbeiner 2011), which we use for the calculation of absolute magnitudes.

Adopting only Milky Way extinction, the absolute magnitude of the source faded from $M_g \simeq -17.1$ and $M_r \simeq -16.8$ at discovery to our PS observations at 2.3 days of $M_g \simeq -15.3$, $M_r \simeq -15.8$, $M_i \simeq -15.8$, and $M_z \simeq -16.2$. The full optical light curves, in absolute magnitudes, are presented in Figures 5 and 6.

From just the first few epochs of data, the evolution of SN2025ulz qualitatively resembles the evolution of the KN AT2017gfo (see Figure 6 and Section 5.6). It is around 1 mag brighter at peak, although it was discovered earlier compared to the GW trigger than AT2017gfo. With data from just the first 2.5 days in hand, the temporal coincidence with S250818k, and the 3D spatial consistency, an optical counterpart claim was reasonable (V. Karambelkar et al. 2025). However, continued observations with PS reveal an upturn in the light curve after ∼5 days, which is unexpected for any observed or modeled KN. The slow continuous rise for the subsequent ≈15 days resembles an SN light curve.

5.5. Comparison to SNe IIb

The light curve of SN2025ulz begins to rebrighten at a time $t \gtrsim 5$ days from the discovery epoch (see Figure 3) and continues for a further 10 days. The early luminous peak, followed by rapid fading, and the subsequent second rise to a peak ∼15 days postexplosion is reminiscent of SN IIb light-curve behavior. To further investigate this, we compare the multiband light curve of SN2025ulz with well-sampled light curves of the SNe 1993J (*BRI*; M. W. Richmond et al. 1994), 2008ax (*gri*; A. Pastorello et al. 2008), 2011dh (*gri*; I. Arcavi et al. 2011), and 2016gkg (*gri*; I. Arcavi et al. 2017a; L. Tartaglia et al. 2017). We correct all observed photometry for reddening effects before converting to absolute magnitudes, for ease of comparison. For SNe 1993J, 2008ax, 2011dh, and 2016gkg, we consult the above references for extinction corrections, distance, and explosion time estimates. For SN2025ulz, we assume an explosion phase equal to the GW merger time (The LIGO Scientific Collaboration et al. 2025a). This is to show that even if the GW merger time was close to the SN explosion by coincidence, the light curve still resembles a typical SN IIb.

In all *gri* bands, the qualitative evolution of SN2025ulz mirrors SNe 2011dh and 2016gkg. The data resemble the evolution of SN1993J, but it appears that SN2025ulz evolved on a more rapid timescale. It is also very similar to the high-cadence light curves of SN2017jgh and SN2021zby—SNe IIb observed by Kepler and TESS, respectively (P. Armstrong et al. 2021; Q. Wang et al. 2023). However, a direct comparison of SN2025ulz to these two SNe is more

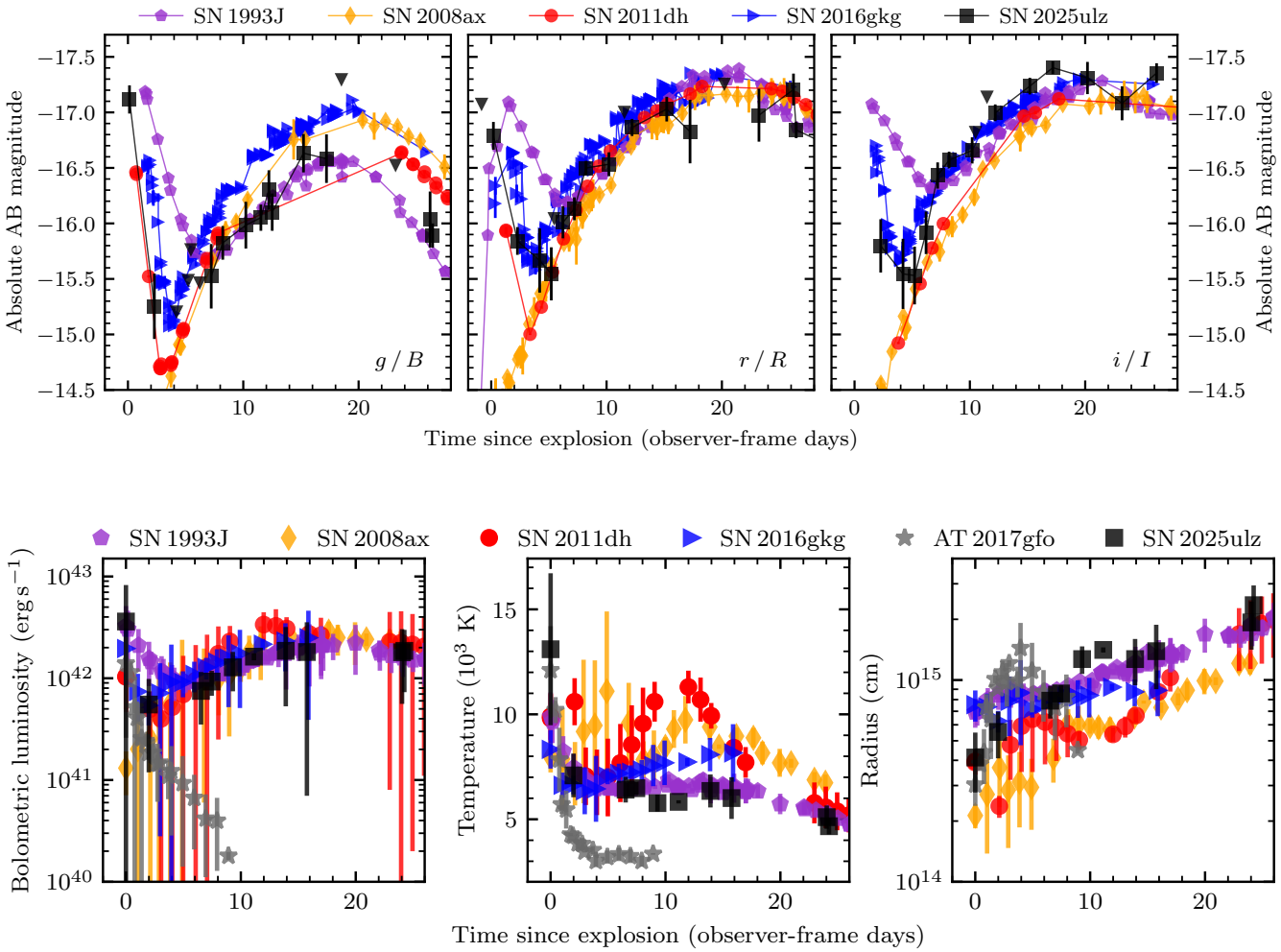

Figure 5. Top: comparison of SN2025ulz *gri*-band evolution to the early light curves of SNe 1993J (*BRI*), 2008ax (*gri*), 2011dh (*gri*), and 2016gkg (*gri*)—all SNe IIb that possess early-time observations. The evolution of SN2025ulz closely resembles the evolution of these transient events. Bottom: bolometric luminosity ($L_{\rm BOL}$) light-curve property comparisons between SN2025ulz and SNe 1993J, 2008ax, 2011dh, and 2016gkg and the KN AT2017gfo. The $L_{\rm BOL}$ evolution of SN2025ulz closely mirrors the comparison sample of SNe IIb, whereas it exhibits a stark difference to that of AT2017gfo. A similar trend exists for the temperature comparison.

challenging, since the Kepler and TESS filters are extremely broad. These shock-cooling tails are common in SNe IIb, but vary in their duration and peak luminosity (B. Ayala et al. 2025), and are modeled with extended envelopes of modest mass (e.g., I. Arcavi et al. 2017a; A. L. Piro et al. 2017). In some cases, such as SN2008ax, no shock-cooling signature is observed. The absolute magnitudes of all comparison SNe agree well with SN2025ulz; both in the ^{56}Ni-powered main peak as well as in the initial sharp decline. The evolutionary timescales (SN1993J aside) also agree well. From this visual inspection, it is clear that, based on photometry alone, the photometric data can be well explained by SN2025ulz being a typical SN IIb. Furthermore, despite only correcting for Milky Way extinction, the data of SN2025ulz closely match these comparison events. This indicates that host galaxy extinction for SN2025ulz may be minor.

To further quantify the agreement between SN2025ulz and our sample of comparison SNe IIb, we fit the photometry of each event with `SuperBol` (M. Nicholl 2018), to extract bolometric luminosity ($L_{\rm BOL}$) light-curve properties. In Figure 5, we compare the bolometric light curves and photospheric temperatures and radii extracted for SN2025ulz with those of SNe 1993J, 2008ax, 2011dh, and 2016gkg, as well as the KN AT2017gfo. We find that the $L_{\rm BOL}$ evolution of SN2025ulz closely matches all comparison SNe. The evolution of AT2017gfo is starkly different, plummeting in luminosity much faster than any of the SNe. A similar trend is found for temperature evolution. While there is some scatter among the population of SNe IIb (and SN2025ulz), the evolution of AT2017gfo is again distinct, as it exhibits much more rapid cooling than any of these other events. These $L_{\rm BOL}$ comparisons again unambiguously demonstrate the similarities between SN2025ulz and SNe IIb, while also highlighting the differences with the KN AT2017gfo (see Section 5.6 for more comparison to AT2017gfo).

The SNIFS observation described in Section 5.3 was centered on the position of SN2025ulz, and excess flux is visible at the transient position in the collapsed white-light B and R cubes, offset from the galaxy core. The seeing was excellent (0.″6–0.″8), and the SNIFS spaxals subtend 0.″43. We extracted a spectrum within a 0.8 spaxal radius of the SN2025ulz position. The spectrum (taken 15 days post-GW-signal; see Figure 4) possesses broad absorption to the blue of Hα, which likely corresponds to P Cygni absorption from SN2025ulz, as described in the spectroscopic classification report of SN2025ulz as an SN of type II or IIb (S. Banerjee et al. 2025b). The velocities are consistent between the VLT+MUSE spectrum (S. Banerjee et al. 2025b) and our SNIFS spectrum, indicating a velocity for the P Cygni trough of $v_{\rm ej} \simeq 14{,}000$ km s^{-1}. This is fairly typical for an SN IIb,

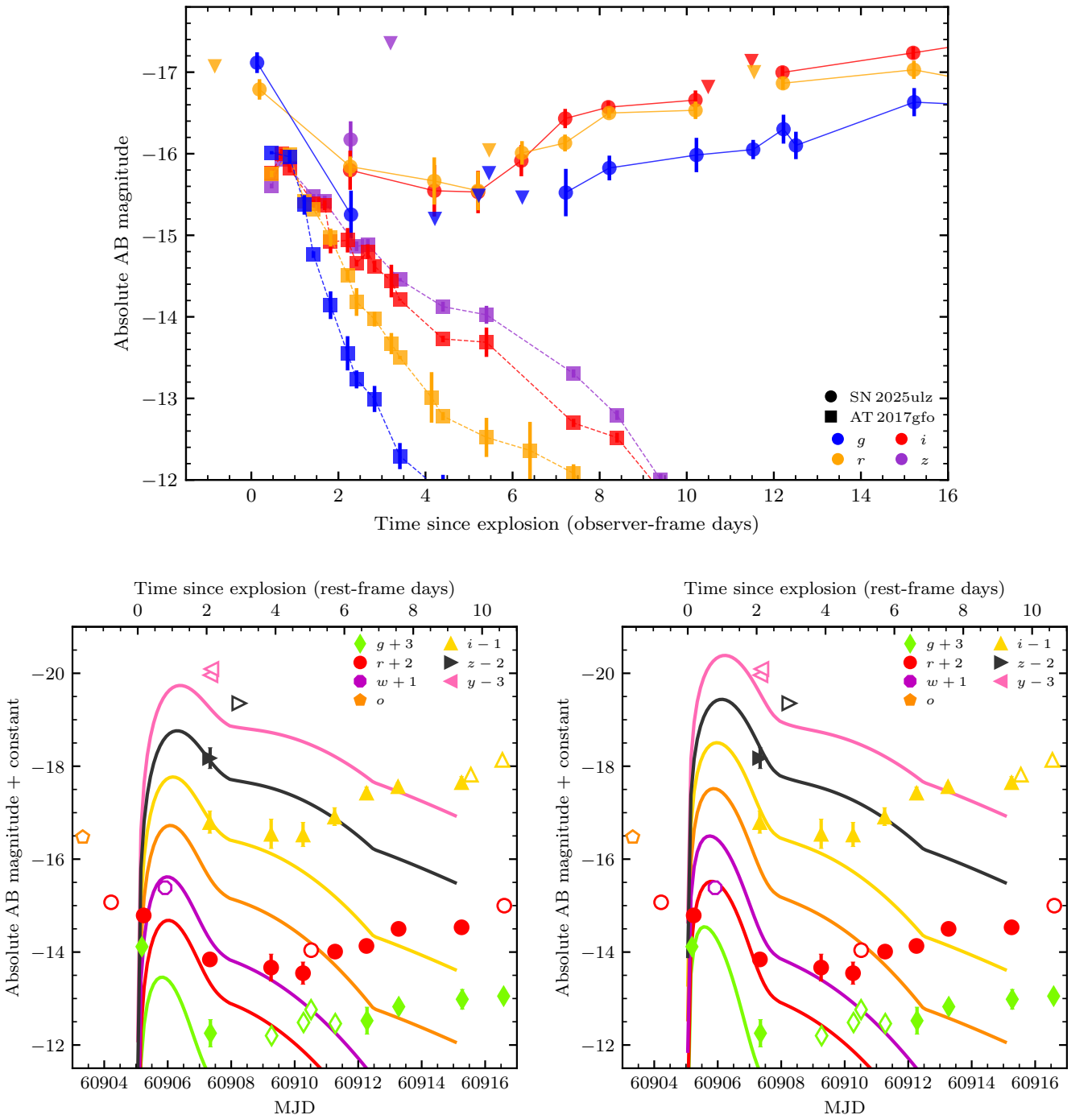

Figure 6. Top: comparison of the *griz*-band light curves of SN2025ulz and AT2017gfo. The downward-facing triangles correspond to 3σ upper limits for SN2025ulz. Bottom: KN model fits for SN2025ulz. Both models presented have dynamical (low-opacity) ejecta, with 0.025 $M_\odot$ and 0.3c, and disk wind (higher-opacity) ejecta, with 0.05 $M_\odot$ and 0.15c. The model on the left possesses no shock heating, whereas the model on the right is generated invoking maximum shock heating. The hollow symbols correspond to 3σ upper limits.

with SN2011dh showing Hα absorption trough minima at velocities of 16,000–13,000 km s^{-1} between explosion and 15 days (M. Ergon et al. 2014). We suggest that the consistency between the ENGRAVE collaboration's spectral typing and our SNIFS spectrum rules out SN2025ulz being a KN and favors an SN of type IIb.

5.6. Comparison to AT2017gfo

To further demonstrate the incompatibility of a KN interpretation, we compare the optical *griz*-band light curve of SN2025ulz with AT2017gfo. Specifically, we compare to the optical data from I. Andreoni et al. (2017), I. Arcavi et al. (2017b), R. Chornock et al. (2017), P. S. Cowperthwaite et al. (2017), M. R. Drout et al. (2017), P. A. Evans et al. (2017), M. M. Kasliwal et al. (2017), E. Pian et al. (2017), S. J. Smartt et al. (2017), N. R. Tanvir et al. (2017), E. Troja et al. (2017), Y. Utsumi et al. (2017), and S. Valenti et al. (2017), compiled by M. W. Coughlin et al. (2018).[22] As above, we correct the

[22] This photometry data file is available at www.engrave-eso.org.

data for reddening effects, before converting into absolute magnitudes (assuming a distance of 40.4 Mpc; J. Hjorth et al. 2017). This comparison is plotted in Figure 6.

The rapid decline from the *gr*-band ZTF discovery points to the first *griz*-band data from PS at 2.3 days post-GW-trigger is not as fast as that observed for AT2017gfo at the same phases (although it is somewhat comparable; see Section 5.4). SN2025ulz is 0.5–1 mag brighter than AT2017gfo in both g and r at $\sim$0.5 days postexplosion. Beyond $\approx$2.3 days, AT2017gfo continues to evolve on a rapid timescale across all *griz* bands, whereas SN2025ulz flattens. The rebrightening in the *gri*-band data of SN2025ulz is irrefutable after $\approx$6 days, at which point SN2025ulz is $\gtrsim$2.5 mag brighter in i band (the discrepancy is even larger in the *gr* bands). Clearly, the evolution of SN2025ulz does not match that of AT2017gfo beyond a few days. This is also clear from our $L_{\rm BOL}$ light-curve comparisons in Figure 5. However, KNe are expected to exhibit a diverse range of observational properties and, as such, one cannot formally rule out the KN interpretation, given the data do not exactly match AT2017gfo. Thus, we undertake a modeling approach to see if the light curve of SN2025ulz can be reproduced by a KN.

5.7. Fiducial KN Model

As noted by R. Stein et al. (2025), M. Busmann et al. (2025), and X. J. Hall et al. (2025), and shown in Figure 3, the early emission from SN2025ulz indicated rapid fading, which could be consistent with expectations for a KN. We now consider whether any plausible KN model could fit the observed optical light curve. We explore whether a KN interpretation can be excluded based only on the first few detections (similar to the events discussed in Section 4), whether full light-curve monitoring is necessary, or whether spectroscopy (unambiguously identifying SN2025ulz as an SN) is the only way to rule out a KN in this instance.

We attempted to model the light curve from PS, along with the ZTF discovery points, using the `Modular Open Source Fitter for Transients` (`MOSFiT`; J. Guillochon et al. 2018). We use the analytic (Arnett-like; W. D. Arnett 1982) radioactively heated KN model from B. D. Metzger (2017), as implemented by V. A. Villar et al. (2017), with additional luminosity from shock cooling (following A. L. Piro & J. A. Kollmeier 2018 and M. Nicholl et al. 2021). This is the same model used by J. C. Rastinejad et al. (2022) to analyze the KN associated with GRB 211211A. Applying this to SN2025ulz, we were unable to find a converged model that gives a reasonable fit to the full light curve, trivially confirming that the source is not a KN. Next, we build a fiducial model to match the early peak to demonstrate when the data and models diverge.

We use a two-component ejecta: "blue," with opacity $\kappa_{\rm b} = 0.5\,{\rm cm^2\,g^{-1}}$ and velocity $0.3c$, and "purple," with opacity $\kappa_{\rm p} = 3\,{\rm cm^2\,g^{-1}}$ and velocity $0.15c$. These roughly correspond to the dynamical (blue) and disk wind (purple) ejecta found in the `MOSFiT` fits to AT2017gfo (V. A. Villar et al. 2017; M. Nicholl et al. 2021). These two components dominate the luminosity on timescales of $\sim$1 day and $\sim$1 week, respectively. To reproduce the fast fade between the first detection from ZTF and our earliest PS observation, a blue ejecta mass of $\approx 0.025\,M_\odot$ is required. This is comparable to the mass inferred for AT2017gfo. We also assume a purple ejecta mass of $0.05\,M_\odot$, based on AT2017gfo.

The results are shown in Figure 6. With only r-process heating, the model luminosity falls short of the initial ZTF detections by 1–2 mag but provides a reasonable match to the PS data (particularly in the redder bands) 2 days later. With the addition of shock heating, we can also match the early blue emission. Doing so requires setting the parameter `shock_frac` $= 1$; i.e., all the dynamical ejecta are heated by a strong shock, which could for example result from a GRB jet punching through KN ejecta (A. L. Piro & J. A. Kollmeier 2018). Analysis of AT2017gfo with a binary-constrained KN model (i.e., ejecta mass is determined by the masses of the constituent NSs) also showed evidence for shock heating (M. Nicholl et al. 2021), though with a lower `shock_frac` $\approx$ 0.5. The early UV emission from GRB 211211A suggested a `shock_frac` $= 0.6$–1, though that event had an unusually long-lived GRB jet. In summary, the optical light curve of SN2025ulz during the first 2 days is consistent with a KN model that is perhaps somewhat extreme, but compatible with previous KN models.

However, the model is unable to account for the flattening and subsequent rebrightening of the light curve at later times. While the purple component can produce emission on longer timescales, visible as a bump in the model light curves at $\sim$3–5 days, increasing the mass of this slower, redder component would also increase the luminosity on day two and exceed the observed brightness in the redder bands (i, z, and especially y). Adding an extremely long-lived and redder component (which could arise from tidal ejecta in an asymmetric binary) to try to reproduce the slow rise would require an unrealistic ejecta mass (possibly orders of magnitude larger than in AT2017gfo and outside the range where the `MOSFiT` model is valid). We conclude that no reasonable KN model could reproduce the light-curve evolution beyond $\sim$5 days.

5.8. Host Galaxy Spectral Energy Distribution and Modeling

SN2025ulz is associated with the galaxy WISEA J155154.15 +305409.2, with coordinates R.A. = 15:51:54.156, decl. = +30:54:09.24. To characterize the host galaxy, we make use of the `HostPhot` tool (T. Müller-Bravo & L. Galbany 2022), which extracts consistent multiband photometry from archival surveys. We obtain cutouts from PS, SDSS, Legacy Survey, the Galaxy Evolution Explorer (GALEX), the Two Micron All Sky Survey (2MASS), and unWISE, covering rest-frame wavelengths from the far-UV through the mid-IR. A minimum error floor of 0.05 mag was added in quadrature to account for calibration systematics, and galactic foreground extinction was corrected.

We then modeled the host galaxy spectral energy distribution (SED) using the `Prospector` package (B. D. Johnson et al. 2021). We assumed a Chabrier initial mass function (G. Chabrier 2003), the Milky Way extinction law (J. A. Cardelli et al. 1989), and enable the inclusion of circumstellar dust emission from asymptotic-giant-branch stars. The adopted model is a parametric delayed-τ star formation history (SFH $\propto te^{-t/\tau}$), with free parameters for the total mass formed (M_F), age of the galaxy ($t_{\rm age}$), e-folding timescale (τ), and metallicity (Z). Because $t_{\rm age}$ represents only the onset of star formation, a more physically meaningful measure of stellar population age is the mass-weighted age ($t_{\rm MWA}$), defined as

$$t_{\rm MWA} = t_{\rm age} - \frac{\int_0^{t_{\rm age}} t \cdot {\rm SFH}(t)\,dt}{\int_0^{t_{\rm age}} {\rm SFH}(t)\,dt} \quad (3)$$

(see A. E. Nugent et al. 2020). Similarly, the relevant mass to report is the surviving stellar mass ($M_\star$)—i.e., the

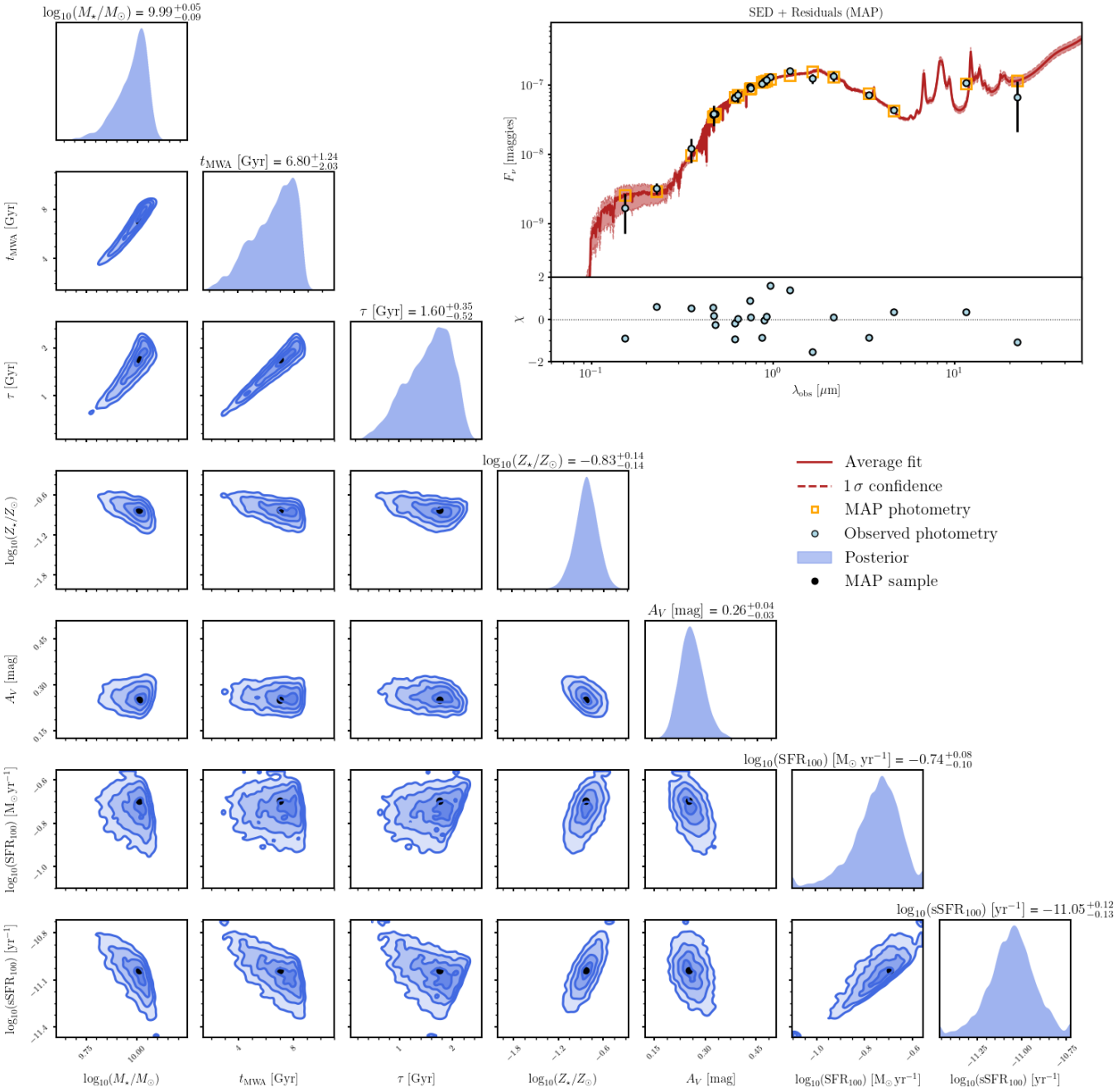

Figure 7. Results of our `Prospector` fit to the broadband SED of the host galaxy of SN2025ulz. The main panel presents the posterior distributions for key stellar population parameters, including the surviving stellar mass (M_* [$M_\odot$]), mass-weighted age ($t_{\rm MWA}$ [Gyr]), star formation timescale (τ [Gyr]), metallicity (Z [$Z_\odot$]), dust attenuation (A_V [AB mag]), and both average star formation rate (SFR$_{100}$ [$M_\odot$ yr^{-1}]) and specific star formation rate (sSFR$_{100}$ [yr^{-1}]) over the past 100 Myr. The contours correspond to 1σ, 2σ, and 3σ confidence intervals, and the quoted values represent the median values and 1σ uncertainties. The inset panel shows the observed photometry (blue points), the maximum a posteriori (MAP) model photometry (orange squares), and the best-fitting model SED (red curve) with 1σ confidence interval (shaded). Residuals relative to the MAP model are also shown.

present-day mass retained in stars and stellar remnants, rather than the total mass formed. This accounts for stellar mass loss over time and can be approximated as

$$M_* \approx M_F \cdot 10^{(1.06-0.24\log_{10}[t_{\rm MWA}({\rm yr})]+0.01\log^2_{10}[t_{\rm MWA}({\rm yr})])} \quad (4)$$

(see J. Leja et al. 2013). Sampling was performed using the `dynesty` nested sampler (J. S. Speagle 2020), providing robust posterior distributions. Stellar population synthesis models are constructed using `fsps` and `Python-fsps` (C. Conroy et al. 2009; C. Conroy & J. E. Gunn 2010). The resulting best-fit SED—along with photometry and residuals—is shown in Figure 7.

From this modeling, we infer the following host galaxy properties:

1. *Stellar mass.* $\log_{10}(M_*/M_\odot) = 9.99^{+0.05}_{-0.09}$
2. *Mass-weighted age.* $t_{\rm MWA}$ (Gyr) $= 6.80^{+1.24}_{-2.03}$

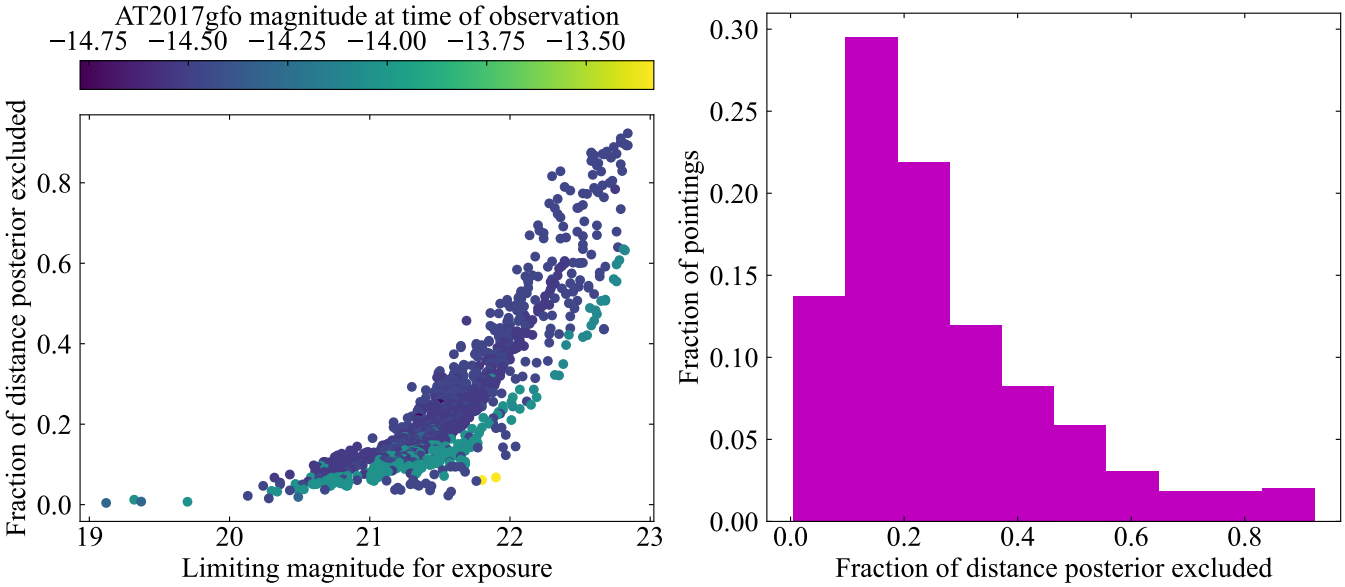

Figure 8. Left: illustration of the limiting magnitude reached by each PS pointing and the corresponding fraction of the distance posterior for which AT2017gfo-like KN emission can be ruled out. Right: histogram highlighting the fraction of pointings that rule out different fractions of the distance posterior of S250818k. Only a few of the pointings enable the ruling out of a substantial fraction ($\gtrsim$0.8) of the distance posterior.

3. *Star formation timescale.* τ (Gyr) $= 1.60^{+0.35}_{-0.52}$
4. *Metallicity.* $\log_{10}(Z/Z_{\odot}) = -0.83^{+0.14}_{-0.14}$
5. *Dust extinction.* $A_V = 0.26^{+0.04}_{-0.03}$
6. *Star formation rate (averaged over the past 100 Myr).* $\log_{10}(\mathrm{SFR}_{100}\,[M_{\odot}\ \mathrm{yr}^{-1}]) = -0.74^{+0.08}_{-0.10}$

Next, we compare these values to the host galaxy of AT2017gfo. GW170817/AT2017gfo occurred in the sd0 galaxy NGC 4993 (J. Hjorth et al. 2017; A. J. Levan et al. 2017). H. F. Stevance et al. (2023) estimated a stellar mass $\log_{10}(M_*/M_{\odot}) = 10.4$ and a dominant stellar population older than 5 Gyr (peaking around 7–12.5 Gyr) with metallicity $Z = 0.010$. A younger stellar component (1 Gyr) with enhanced metal content ($Z = 0.020$–0.030) was found to account for roughly 5% of the total mass of NGC 4993. From our host galaxy modeling of WISEA J155154.15+305409.2, we find similar galaxy ages and masses to those of NGC 4993, but a substantially lower metallicity ($\sim$15 versus 70% solar metallicity).

SN2025ulz is located 0.″88 from its host galaxy, which, at a distance of $\approx$401 Mpc (see Section 5.3), corresponds to a projected physical offset of 1.45 kpc. This is comparable to AT2017gfo, which had a projected distance from NGC 4993 of 1.96 kpc (A. J. Levan et al. 2017).

S. Schulze et al. (2021) present an overview of SN host galaxy properties, including those of SNe IIb. They measure median (mode) galaxy masses of $\log_{10}(M_*/M_{\odot}) = 9.53^{+0.15}_{-0.16}$ $(10.04^{+0.15}_{-0.42})$, ages of 2.2 ± 0.3 $(5.5^{+0.8}_{-0.7})$ Gyr, star formation rates of $\log_{10}(\mathrm{SFR}\ [M_{\odot}\ \mathrm{yr}^{-1}]) = -0.30 \pm 0.12$ $(-0.18^{+0.25}_{-0.29})$, and offsets of $2.70 \pm 0.45(4.06 \pm 0.44)$ kpc. P. L. Kelly & R. P. Kirshner (2012) present metallicity measurements for core-collapse SN host galaxies; they measure a median host galaxy metallicity for SNe IIb of $Z \approx 0.02$. WISEA J155154.15+305409.2 matches the modal values of host galaxy mass and age while possessing a lower-than-average metallicity and star formation rate. We note, however, that metallicity estimates derived from SED fitting to broadband photometry alone are highly uncertain and should be interpreted with caution, as they are generally not well constrained without spectroscopic information. Additionally, the host galaxy offset appears to be lower than average for SNe IIb.

6. Limits on KN Emission from PS Observations

With our multinight pointings from PS, we do not identify any convincing candidate counterparts to S250818k. Next, we investigate whether our observations can constrain the presence of KN emission within the region tiled by PS.

For every PS pointing, we extract an observation time relative to the GW trigger and the 3.5σ limiting magnitude. We then extract the absolute magnitude of the KN model for AT2017gfo from M. Nicholl et al. (2021) at the same time, and in the same filter. This absolute magnitude estimate for AT2017gfo was used to compute a distance at which it would have the same value as the limiting magnitude of each pointing (accounting for line-of-sight extinction). With this distance, we compute the fraction of the distance posterior of S250818k from the `bilby.fits` sky map that can be ruled out along that line of sight—i.e., we integrate the posterior over all distances closer than the distance computed for AT2017gfo to remain at least as bright as our limiting magnitude.

The results of this analysis are plotted in Figure 8. Here, the fraction of posterior distance excluded is plotted against the limiting magnitude of each pointing. From this plot, we can glean a number of useful insights. First, some of the PS pointings reach limiting magnitudes of $\lesssim$22.5, which allow us to rule out an AT2017gfo-like signal across $\gtrsim$80% of the distance posterior. Second, there is a spread in the fraction of the distance posterior excluded for pointings with similar limiting magnitudes. This can be explained by some combination of differences in the distance posterior along different lines of sight, differences in extinction, and the expected magnitude at the time of observation. The data are color-coded to indicate what magnitude AT2017gfo would possess at the same phase as the PS pointings—i.e., the distributions of blue, turquoise, and yellow points essentially

correspond to AT2017gfo at ∼2.2, ∼3.2, and ∼4.2 days postburst. From this, one can see that the pointings from 2025 August 20 (MJD 60907.3; ∼2.2 days postburst) are substantially more constraining than those from even just one day later. This visually illustrates how important rapid follow-up of GW localizations can be.

Also in Figure 8, we present a histogram that visualizes the fraction of pointings that rule out different fractions of distance posterior. A few of the pointings are quite discriminatory, ruling out $>60\%$ of the distance posterior. However, the bulk of our pointings are much less constraining, with the most common result being that we rule out just 10%–20% of the distance posterior.

With the above information, we also compute the fraction of the total surveyed volume within which we can confidently rule out the presence of an AT2017gfo-like signal; we estimate this to be ≈27%. Considering the full `bilby.fits` sky volume, this coverage equates to ≈9.1% of the total 90% sky localization volume. However, we note that if our observations were undertaken when the KN had $M_i = -15.7$ (the brightness of AT 2017gfo at +12 hr), we would be able to rule out the presence of a KN signal across 82% of our surveyed volume. This substantial increase again highlights the paramount importance of expedient follow-up observations.

7. Summary and Conclusions

Here, we have presented our observational campaign following the reported subthreshold GW event S250818k. After establishing that many of the GW signal properties agreed well with astrophysically real GW signals, we outlined our observations tiling the `bilby.fits` sky map with Pan-STARRS and ATLAS. Despite discovering 47 new extragalactic transient phenomena, further observations and analysis ruled all were unrelated to S250818k.

We next presented our follow-up observations of SN2025ulz—a reported candidate counterpart to S250818k. We measured a host galaxy redshift of $z = 0.0849 \pm 0.0003$, which places SN2025ulz (just) within the 2σ LVK distance estimate. Although the initial observations ($\lesssim$4 days) mirror a KN-like decline, the light curve rebrightens after 5 days, more akin to an SN. We compared the full light curve of SN2025ulz to a sample of SNe IIb and found good agreement in early evolution. We also compared to AT2017gfo and KN models and determined that after $\lesssim$5 days, the data are incompatible with a KN interpretation.

Finally, we explored how much of the S250818k `bilby.fits` sky volume we can exclude possessing a AT2017gfo-like transient from our PS follow-up observations. We can exclude ≈27% of the distance posterior covered by PS or ≈9.1% of the total `bilby.fits` 90% sky localization volume. Were our observations executed more quickly (+12 hr, when AT2017gfo possessed $M_i = -15.7$), we would exclude a AT 2017gfo-like transient within 82% of the distance posterior covered by PS. Clearly, rapid follow-up observations are key to providing the best chance of detecting KN emission in future GW sky searches.

Acknowledgments

S.J.S., S.S., K.S., D.Y., J.H.G., F.S., and J.W.T. acknowledge funding from STFC grants ST/Y001605/1, ST/X001253/1, and ST/Y509474/1, a Royal Society Research Professorship, a Royal Society Newton International Fellowship, and the Hintze Family Charitable Foundation. T.-W.C. and A.A. acknowledge the financial support from the Yushan Fellow Program by the Ministry of Education, Taiwan (MOE-111-YSFMS-0008-001-P1), and the National Science and Technology Council, Taiwan (NSTC grant 114-2112-M-008-021-MY3). This work was funded by ANID, Millennium Science Initiative, ICN12_009. Pan-STARRS is primarily funded to search for near-Earth asteroids through NASA grants NNX08AR22G and NNX14AM74G. The Pan-STARRS science products for LIGO–Virgo–KAGRA follow-up are made possible through the contributions of the University of Hawaii's Institute for Astronomy and Queen's University Belfast. Parts of this research were supported by the Australian Research Council Centre of Excellence for Gravitational Wave Discovery (OzGrav), through project No. CE230100016.

The Pan-STARRS1 Sky Surveys have been made possible through contributions by the University of Hawaii's Institute for Astronomy, the Pan-STARRS Project Office, the Max Planck Society and its participating institutes, the Max Planck Institute for Astronomy, Heidelberg, and the Max Planck Institute for Extraterrestrial Physics, Garching, Johns Hopkins University, Durham University, the University of Edinburgh, Queen's University Belfast, the Harvard–Smithsonian Center for Astrophysics, the Las Cumbres Observatory Global Telescope Network Incorporated, the National Central University of Taiwan, the Space Telescope Science Institute, the National Aeronautics and Space Administration under grant No. NNX08AR22G issued through the Planetary Science Division of the NASA Science Mission Directorate, the National Science Foundation grant No. AST-1238877, the University of Maryland, Eotvos Lorand University, and the Los Alamos National Laboratory. This work has made use of data from the Asteroid Terrestrial-impact Last Alert System project. ATLAS is primarily funded to search for near-Earth asteroids (NEOs) through NASA grants NN12AR55G, 80NSSC18K0284, and 80NSSC18K1575; by-products of the NEO search include images and catalogs from the survey area. The ATLAS science products have been made possible through the contributions of the University of Hawaii's Institute for Astronomy, Queen's University Belfast, the Space Telescope Science Institute, and the South African Astronomical Observatory. This publication makes use of data collected at Lulin Observatory, which is partly supported by the TAOVA grant NSTC 114-2740-M-008-002.

This research has made use of the NASA/IPAC Extragalactic Database (NED), which is operated by the Jet Propulsion Laboratory, California Institute of Technology, under contract with the National Aeronautics and Space Administration.

Data Availability

The updated PS reference images utilized for accurate difference imaging of SN2025ulz (see Section 5.1) are publicly available at 624c1bc5-b841-4da0-9c56-c8683454da7f

Facilities: PS1, ATLAS, LO:1m, LO:0.4m, UH:2.2m (SNIFS).

Software: Astropy (Astropy Collaboration et al. 2013, 2018, 2022), Scipy (P. Virtanen et al. 2020), MOSFiT (J. Guillochon et al. 2018), Photutils (L. Bradley et al. 2022).

Table 1
Pan-STARRS Candidate Counterpart Discoveries

PS Name	IAU TNS Name	R.A.	Decl.	Discovery (MJD)	Discovery AB (mag)	Discovery Filter	Redshift (z)	Comments
PS25grz	AT2025uso	16:16:57.43	+35:03:21.0	60907.361	20.47 ± 0.18	*i*	0.025^{s} (DESI DR1)	Outside final `bilby.fits` sky map. SN LC in ATLAS.
PS25gsa	AT2025usy	17:55:12.50	+56:02:02.0	60907.375	20.95 ± 0.27	*i*	0.090 ± 0.012^{p} (LS)	Flat LC. Beyond 2σ LVK limit.
PS25gsh	AT2025utr	18:07:46.73	+56:52:12.8	60907.417	19.84 ± 0.13	*i*	0.043 ± 0.011^{p} (LS)	SN LC in ATLAS.
PS25gsm	AT2025utx	16:44:10.88	+42:27:55.1	60907.421	20.21 ± 0.26	*i*	0.080^{s} (DESI DR1)	Flat LC. Too bright ($M_i \sim -17.6$).
PS25gsv	AT2025uuf	20:40:40.26	+64:36:41.4	60907.377	20.99 ± 0.29	*i*	0.061^{p} (2MASS)	Flat LC.
PS25gtm	AT2025uuw	16:36:55.61	+44:22:48.1	60907.373	20.44 ± 0.20	*i*	0.034 ± 0.006^{p} (LS)	Classified as an SN Ia.
PS25guo	AT2025uxs	15:44:14.34	+27:28:41.9	60909.291	20.05 ± 0.08	*i*	0.063^{s} (DESI DR1)	SN LC in ATLAS.
PS25grv	AT2025usk	16:04:49.18	+35:47:26.8	60907.355	20.81 ± 0.29	*i*	0.229 ± 0.039^{p} (LS)	Too distant.
PS25grw	AT2025usl	15:48:34.68	+32:17:37.6	60907.300	21.57 ± 0.24	*g*	0.218 ± 0.282^{p} (LS)	Likely a CV. Alternatively,
”	”	”	”	”	”	”	0.050^{s} (SDSS)	offset from galaxy at $z = 0.05$, but flat LC.
PS25grx	AT2025usm	15:47:43.01	+30:32:53.5	60907.309	21.69 ± 0.25	*r*	0.319 ± 0.069^{p} (LS)	Too distant.
PS25gry	AT2025usn	15:50:27.14	+30:20:01.2	60907.298	21.05 ± 0.15	*g*	0.217^{s} (DESI DR1)	Too distant.
PS25gsg	AT2025utq	17:31:46.85	+54:47:47.6	60907.374	20.12 ± 0.15	*i*	0.075 ± 0.011^{p} (LS)	Flat LC. Too bright ($M_i \sim -18$).
PS25gsi	AT2025utt	17:50:21.38	+54:57:56.2	60907.375	20.34 ± 0.20	*i*	0.269^{s} (DESI DR1)	Too distant.
PS25gsj	AT2025utu	20:07:56.23	+61:20:47.4	60907.412	20.81 ± 0.16	*i*	0.169 ± 0.020^{p} (SDSS)	Too distant.
PS25gsk	AT2025utv	17:15:00.36	+51:22:01.3	60907.373	20.01 ± 0.14	*i*	0.105 ± 0.068^{p} (LS)	Flat LC.
PS25gsl	AT2025utw	19:47:51.84	+64:30:33.0	60907.425	20.59 ± 0.23	*i*	0.899 ± 0.544^{p} (LS)	Too distant.
PS25gsn	AT2025uty	17:41:51.38	+52:25:50.3	60907.408	20.74 ± 0.23	*i*	0.646 ± 0.204^{p} (LS)	Too distant.
PS25gso	AT2025utz	16:31:07.87	+40:42:44.0	60907.357	20.70 ± 0.30	*i*	0.279 ± 0.032^{p} (LS)	Too distant.
PS25gsp	AT2025uua	17:25:45.69	+51:55:43.2	60907.373	20.87 ± 0.26	*i*	0.280 ± 0.077^{p} (LS)	Too distant.
PS25gss	AT2025uub	20:01:03.14	+61:58:53.8	60907.396	19.16 ± 0.06	*i*	…	High-proper-motion star.
PS25gst	AT2025uuc	17:39:58.54	+53:20:15.8	60907.411	20.89 ± 0.31	*i*	$0.305 \pm 0.109/0.158 \pm 0.201^{p}$ (LS)	Either too distant or a likely CV.
PS25gsu	AT2025uud	20:53:53.82	+65:10:57.2	60907.450	20.06 ± 0.12	*i*	…	Flat LC. Possibly Galactic.
PS25gsx	AT2025uug	19:02:03.80	+59:19:37.5	60907.376	20.64 ± 0.15	*i*	0.145 ± 0.022^{p} (LS)	Too distant.
PS25gsy	AT2025uuh	18:54:47.78	+60:12:28.0	60907.488	21.48 ± 0.28	*i*	0.456 ± 0.459^{p} (LS)	Flat LC. Very uncertain redshift.
PS25gsz	AT2025uui	15:58:55.23	+30:59:35.9	60907.304	20.86 ± 0.19	*g*	0.174^{s} (DESI DR1)	Too distant.
PS25gta	AT2025uuk	17:29:35.00	+54:36:16.3	60907.374	20.30 ± 0.24	*i*	0.202 ± 0.006^{p} (LS)	Too distant.
PS25gtc	AT2025uuo	17:11:33.53	+51:33:37.2	60907.373	20.04 ± 0.19	*i*	0.128 ± 0.008^{p} (LS)	Too distant.
PS25gtd	AT2025uup	19:50:58.53	+61:33:04.7	60907.396	20.96 ± 0.21	*i*	0.411 ± 0.121^{p} (LS)	Too distant.
PS25gte	AT2025uuq	16:18:35.31	+37:56:33.2	60907.363	20.21 ± 0.24	*i*	0.148 ± 0.028^{p} (LS)	Too distant.
PS25gtf	AT2025uur	15:47:00.15	+30:31:38.2	60907.298	21.87 ± 0.35	*g*	0.294 ± 0.111^{p} (LS)	Too distant.
PS25gtg	AT2025uus	16:17:10.71	+39:38:55.0	60907.357	20.83 ± 0.27	*i*	0.142 ± 0.018^{p} (LS)	Too distant.
PS25gth	AT2025uut	18:54:16.71	+60:01:57.4	60907.396	20.81 ± 0.22	*i*	0.093 ± 0.030^{p} (LS)	Flat LC.
PS25gti	AT2025uuu	17:48:26.47	+56:00:47.8	60907.375	21.32 ± 0.29	*i*	0.374 ± 0.088^{p} (LS)	Too distant.
PS25gtj	AT2025uuv	20:46:53.44	+65:07:37.0	60907.432	20.67 ± 0.27	*i*	…	No redshift. Flat LC out to MJD 60924.3.
PS25gtt	AT2025uvs	17:56:55.28	+55:21:05.5	60907.375	21.24 ± 0.27	*i*	1.211^{s} (DESI DR1)	Too distant.
PS25gtu	AT2025uvt	15:55:32.44	+31:00:35.1	60907.323	22.16 ± 0.32	*i*	2.710^{s} (DESI DR1)	Too distant.
PS25gtv	AT2025uvu	15:46:51.46	+29:59:58.0	60907.298	21.94 ± 0.29	*g*	0.784^{s} (DESI DR1)	Too distant.
”	”	”	”	”	”	”	Nearby galaxies have $z = 0.112, 0.113^{s}$ (DESI DR1)	Also too distant.
PS25gum	AT2025uxm	15:56:59.45	+29:25:24.5	60907.306	21.82 ± 0.25	*g*	1.350^{s} (DESI DR1)	Too distant.
PS25gun	AT2025uxo	16:35:33.20	+41:00:57.9	60909.301	20.57 ± 0.17	*i*	0.127 ± 0.036^{p} (LS)	Too distant.
PS25guq	AT2025uya	16:34:33.59	+43:57:01.3	60909.272	20.80 ± 0.17	*i*	0.272 ± 0.033^{p} (LS)	Too distant.

Table 1
(Continued)

PS Name	IAU TNS Name	R.A.	Decl.	Discovery (MJD)	Discovery AB (mag)	Discovery Filter	Redshift (z)	Comments
PS25hah	AT2025vjj	15:45:16.27	+29:31:58.6	60912.251	22.05 ± 0.29	*i*	0.112^{s} (DESI DR1)	Too distant.
PS25hcu	AT2025war	19:53:44.05	+60:42:10.6	60907.412	20.44 ± 0.11	*i*	0.144 ± 0.028^{p} (SDSS)	Too distant.
PS25hcv	AT2025wat	16:01:46.84	+31:13:29.9	60913.257	22.38 ± 0.23	*i*	0.419 ± 0.053^{p} (LS)	Too distant.
”	”	”	”	”	”	”	Nearby galaxies have $z = 0.072$, 0.030^{s} (DESI DR1)	SN-like LC evolution.
PS25hdv	AT2025wek	15:48:19.75	+32:45:36.8	60907.302	21.92 ± 0.30	*g*	0.741^{s} (DESI DR1)	Too distant.
PS25hdw	AT2025wel	15:42:57.22	+30:24:56.9	60909.264	22.05 ± 0.30	*i*	0.449 ± 0.067^{p} (LS)	Too distant.
PS25hdx	AT2025wfr	15:50:30.57	+29:21:17.7	60913.250	21.98 ± 0.20	*i*	0.387 ± 0.086^{p} (LS)	Too distant.
PS25hdy	AT2025wfs	15:46:17.15	+31:50:19.8	60910.263	22.22 ± 0.30	*i*	0.266 ± 0.086^{p} (LS)	Too distant.

Notes. LC = light curve.
^{s} = spectroscopically derived redshift. ^{p} = photometrically derived redshift. References: Legacy Surveys (LS) = D. Schlegel et al. (2021); SDSS = D. S. Aguado et al. (2019); DESI DR1 = DESI Collaboration et al. (2025); and 2MASS = M. Bilicki et al. (2014).

Table 2
Observations of SN2025ulz

$t - t_0$ (days)	MJD	Filter	Total Exposure Time (s)	Apparent Magnitude (AB mag)
Pan-STARRS				
−9.737	60895.319	*i*	180	>21.00
−0.823	60904.233	*y*	120	>19.70
2.270	60907.325	*i*	900	22.27 ± 0.24
2.273	60907.329	*r*	1800	22.24 ± 0.12
2.281	60907.337	*z*	900	21.88 ± 0.22
2.290	60907.345	*g*	1800	22.85 ± 0.29
2.307	60907.362	*y*	1800	>21.40
3.193	60908.248	*y*	1800	>19.62
3.198	60908.254	*z*	1800	>20.70
3.215	60908.270	*g*	1800	>21.53
3.218	60908.273	*i*	1350	>21.09
4.202	60909.257	*r*	1200	22.42 ± 0.29
4.203	60909.258	*i*	1800	22.52 ± 0.32
4.216	60909.272	*g*	1200	>22.91
5.206	60910.262	*r*	1800	22.54 ± 0.24
5.208	60910.263	*i*	1800	22.54 ± 0.26
5.223	60910.279	*g*	1800	>22.62
6.201	60911.257	*i*	1800	22.15 ± 0.19
6.217	60911.272	*r*	1800	22.07 ± 0.14
6.223	60911.279	*g*	1800	>22.65
7.205	60912.260	*r*	1800	21.95 ± 0.10
7.208	60912.263	*i*	1800	21.63 ± 0.12
7.222	60912.278	*g*	1800	22.58 ± 0.29
8.200	60913.255	*i*	1800	21.50 ± 0.07
8.216	60913.271	*r*	1800	21.58 ± 0.06
8.223	60913.278	*g*	1800	22.28 ± 0.15
10.200	60915.256	*i*	1800	21.41 ± 0.12
10.201	60915.257	*r*	1800	21.55 ± 0.11
10.223	60915.278	*g*	1800	22.12 ± 0.21
12.200	60917.256	*i*	1800	21.07 ± 0.07
12.210	60917.266	*r*	1800	21.22 ± 0.08
12.222	60917.278	*g*	1800	21.81 ± 0.18
15.201	60920.257	*i*	1800	20.83 ± 0.07
15.216	60920.272	*r*	1800	21.05 ± 0.11
15.223	60920.278	*g*	1800	21.48 ± 0.17
17.192	60922.248	*i*	1800	20.66 ± 0.06
17.215	60922.270	*g*	1800	21.52 ± 0.22
17.237	60922.292	*r*	1800	21.26 ± 0.29
20.197	60925.253	*i*	600	20.76 ± 0.14
20.205	60925.261	*g*	600	>20.37
20.213	60925.269	*r*	600	>20.83
23.197	60928.253	*i*	600	20.98 ± 0.15
23.205	60928.260	*g*	600	>21.59
23.213	60928.268	*r*	600	21.11 ± 0.24
26.190	60931.246	*i*	600	20.71 ± 0.09
26.198	60931.254	*g*	600	22.07 ± 0.25
26.206	60931.262	*r*	600	20.88 ± 0.14
29.184	60934.240	*i*	600	21.13 ± 0.19
29.192	60934.247	*g*	600	>21.82
29.199	60934.255	*r*	600	21.38 ± 0.24
35.189	60940.245	*i*	1800	21.56 ± 0.19
38.179	60943.234	*i*	600	21.75 ± 0.31
38.187	60943.242	*r*	600	>21.87
38.194	60943.250	*g*	600	>21.72
42.171	60947.227	*i*	600	>21.33
42.180	60947.235	*r*	600	>21.98
42.188	60947.243	*g*	600	>21.85
45.172	60950.227	*i*	600	21.55 ± 0.27
45.180	60950.235	*r*	600	>21.52
48.174	60953.230	*i*	600	>21.39
48.182	60953.238	*r*	600	>21.05
52.167	60957.222	*i*	600	21.98 ± 0.30
52.174	60957.230	*r*	600	>21.94
58.160	60963.216	*i*	600	>21.41
58.169	60963.225	*r*	600	>21.37
62.159	60967.214	*i*	1200	>20.91
ATLAS				
−1.734	60903.322	*o*	440	>21.60
0.860	60905.916	*w*	120	>21.70
LOT				
5.459	60910.515	*g*	900	>22.35
5.463	60910.518	*r*	900	>22.04
5.531	60910.587	*u*	1800	>21.14
11.526	60916.582	*g*	1800	22.06 ± 0.12
11.547	60916.602	*r*	1500	>21.08
12.507	60917.563	*g*	1800	22.01 ± 0.17
18.511	60923.567	*g*	1800	>20.82
26.419	60931.475	*g*	1800	22.22 ± 0.11
26.441	60931.497	*r*	1800	21.24 ± 0.07
SLT				
10.493	60915.548	*i*	7200	>21.25
11.487	60916.542	*i*	2400	>20.93
28.445	60933.501	*i*	3600	>21.05

Note. Here, t_0 denotes the time reported for the GW event (MJD 60905.055625; The LIGO Scientific Collaboration et al. 2025a). Magnitudes are not corrected for the expected foreground extinction of $E(B - V) = 0.0244$ (E. F. Schlafly & D. P. Finkbeiner 2011). Limiting magnitudes are quoted to 3σ significance.

ORCID iDs

J. H. Gillanders https://orcid.org/0000-0002-8094-6108
M. E. Huber https://orcid.org/0000-0003-1059-9603
M. Nicholl https://orcid.org/0000-0002-2555-3192
S. J. Smartt https://orcid.org/0000-0002-8229-1731
K. W. Smith https://orcid.org/0000-0001-9535-3199
K. C. Chambers https://orcid.org/0000-0001-6965-7789
D. R. Young https://orcid.org/0000-0002-1229-2499
J. W. Tweddle https://orcid.org/0009-0004-5681-545X
S. Srivastav https://orcid.org/0000-0003-4524-6883
M. D. Fulton https://orcid.org/0000-0003-1916-0664
F. Stoppa https://orcid.org/0000-0002-3424-8528
G. S. H. Paek https://orcid.org/0000-0002-6639-6533
A. Aamer https://orcid.org/0000-0002-9085-8187
M. R. Alarcon https://orcid.org/0000-0002-8134-2592
A. Andersson https://orcid.org/0000-0003-2734-1895
A. Aryan https://orcid.org/0000-0002-9928-0369
K. Auchettl https://orcid.org/0000-0002-4449-9152
T.-W. Chen https://orcid.org/0000-0002-1066-6098
T. de Boer https://orcid.org/0000-0001-5486-2747
A. K. H. Kong https://orcid.org/0000-0002-5105-344X
J. Licandro https://orcid.org/0000-0002-9214-337X
T. Lowe https://orcid.org/0000-0002-9438-3617
D. Magill https://orcid.org/0009-0000-6521-8842

E. A. Magnier https://orcid.org/0000-0002-7965-2815
P. Minguez https://orcid.org/0009-0003-8803-8643
T. Moore https://orcid.org/0000-0001-8385-3727
G. Pignata https://orcid.org/0000-0003-0006-0188
A. Rest https://orcid.org/0000-0002-4410-5387
M. Serra-Ricart https://orcid.org/0000-0002-2394-0711
B. J. Shappee https://orcid.org/0000-0003-4631-1149
I. A. Smith https://orcid.org/0000-0001-8605-5608
M. A. Tucker https://orcid.org/0000-0002-2471-8442
R. Wainscoat https://orcid.org/0000-0002-1341-0952

References

Abac, A. G., Abbott, R., Abouelfettouh, I., et al. 2024, ApJL, 970, L34
Abbott, B. P., Abbott, R., Abbott, T. D., et al. 2017a, PhRvL, 119, 161101
Abbott, B. P., Abbott, R., Abbott, T. D., et al. 2017b, ApJL, 848, L13
Abbott, B. P., Abbott, R., Abbott, T. D., et al. 2017c, ApJL, 848, L12
Abbott, B. P., Abbott, R., Abbott, T. D., et al. 2020, ApJL, 892, L3
Abbott, R., Abbott, T. D., Abraham, S., et al. 2020, ApJL, 896, L44
Abbott, R., Abbott, T. D., Abraham, S., et al. 2021, ApJL, 915, L5
Abbott, R., Abbott, T. D., Acernese, F., et al. 2023, PhRvX, 13, 041039
Aguado, D. S., Ahumada, R., Almeida, A., et al. 2019, ApJS, 240, 23
Anand, S., Coughlin, M. W., Kasliwal, M. M., et al. 2021, NatAs, 5, 46
Andreoni, I., Ackley, K., Cooke, J., et al. 2017, PASA, 34, e069
Andreoni, I., Kool, E. C., Sagués Carracedo, A., et al. 2020, ApJ, 904, 155
Arcavi, I., Gal-Yam, A., Yaron, O., et al. 2011, ApJL, 742, L18
Arcavi, I., Hosseinzadeh, G., Brown, P. J., et al. 2017a, ApJL, 837, L2
Arcavi, I., Hosseinzadeh, G., Howell, D. A., et al. 2017b, Natur, 551, 64
Armstrong, P., Tucker, B. E., Rest, A., et al. 2021, MNRAS, 507, 3125
Arnett, W. D. 1982, ApJ, 253, 785
Astropy Collaboration, Price-Whelan, A. M., Lim, P. L., et al. 2022, ApJ, 935, 167
Astropy Collaboration, Price-Whelan, A. M., Sipocz, B. M., et al. 2018, AJ, 156, 123
Astropy Collaboration, Robitaille, T. P., Tollerud, E. J., et al. 2013, A&A, 558, A33
Ayala, B., Anderson, J. P., Pignata, G., et al. 2025, A&A, 701, A128
Banerjee, S., Botticella, M., Brennan, S. J., et al. 2025a, TNSCR, 2025–3373, 1
Banerjee, S., Botticella, M.-T., Brennan, S. J., et al. 2025b, GCN, 41476, 1
Bellm, E. C., Kulkarni, S. R., Graham, M. J., et al. 2019, PASP, 131, 018002
Berger, E., Fong, W., & Chornock, R. 2013, ApJL, 774, L23
Bilicki, M., Jarrett, T. H., Peacock, J. A., Cluver, M. E., & Steward, L. 2014, ApJS, 210, 9
Bradley, L., Sipocz, B., Robitaille, T., et al., 2022 astropy/photutils: v1.5.0, Zenodo, doi:10.5281/zenodo.6825092
Brennan, S. J., & Fraser, M. 2022, A&A, 667, A62
Bulla, M. 2019, MNRAS, 489, 5037
Busmann, M., Hall, X. J., Gruen, D., O'Connor, B., & Palmese, A. 2025, GCN, 41421, 1
Cardelli, J. A., Clayton, G. C., & Mathis, J. S. 1989, ApJ, 345, 245
Chabrier, G. 2003, PASP, 115, 763
Chambers, K. C., Magnier, E. A., Metcalfe, N., et al. 2016, arXiv:1612.05560
Chen, T.-W., Yang, S., Srivastav, S., et al. 2025, ApJ, 983, 86
Chen, Y.-X., & Metzger, B. D. 2025, ApJL, 991, L22
Chornock, R., Berger, E., Kasen, D., et al. 2017, ApJL, 848, L19
Conroy, C., & Gunn, J. E. 2010, ApJ, 712, 833
Conroy, C., Gunn, J. E., & White, M. 2009, ApJ, 699, 486
Coughlin, M. W., Dietrich, T., Doctor, Z., et al. 2018, MNRAS, 480, 3871
Coulter, D. A., Foley, R. J., Kilpatrick, C. D., et al. 2017, Sci, 358, 1556
Cowperthwaite, P. S., Berger, E., Villar, V. A., et al. 2017, ApJL, 848, L17
DESI Collaboration, Abdul-Karim, M., Adame, A. G., et al. 2025, arXiv:2503.14745
Drout, M. R., Piro, A. L., Shappee, B. J., et al. 2017, Sci, 358, 1570
Ergon, M., Sollerman, J., Fraser, M., et al. 2014, A&A, 562, A17
Evans, P. A., Cenko, S. B., Kennea, J. A., et al. 2017, Sci, 358, 1565
Flewelling, H. A., Magnier, E. A., Chambers, K. C., et al. 2020, ApJS, 251, 7
Fremling, C., Neill, D., & Sharma, Y. 2025, TNSCR, 2025–3487, 1
Fulton, M. D., Smartt, S. J., Huber, M. E., et al. 2025, MNRAS, 542, 541
Gillanders, J. H., Huber, M. E., Chambers, K. C., et al. 2025, GCN, 41454, 1
Gillanders, J. H., Troja, E., Fryer, C. L., et al. 2023, arXiv:2308.00633
Guillochon, J., Nicholl, M., Villar, V. A., et al. 2018, ApJS, 236, 6
Hall, X. J., Busmann, M., Gruen, D., O'Connor, B., & Palmese, A. 2025, GCN, 41433, 1
Hjorth, J., Levan, A. J., Tanvir, N. R., et al. 2017, ApJL, 848, L31
Johnson, B. D., Leja, J., Conroy, C., & Speagle, J. S. 2021, ApJS, 254, 22
Karambelkar, V., Kasliwal, M. M., Hall, X. J., et al. 2025, GCN, 41436, 1
Kasen, D., Badnell, N. R., & Barnes, J. 2013, ApJ, 774, 25
Kasen, D., Metzger, B., Barnes, J., Quataert, E., & Ramirez-Ruiz, E. 2017, Natur, 551, 80
Kasliwal, M. M., Nakar, E., Singer, L. P., et al. 2017, Sci, 358, 1559
Kelly, P. L., & Kirshner, R. P. 2012, ApJ, 759, 107
Kilpatrick, C. D., Foley, R. J., Kasen, D., et al. 2017, Sci, 358, 1583
Kouveliotou, C., Meegan, C. A., Fishman, G. J., et al. 1993, ApJL, 413, L101
Lamb, G. P., Tanvir, N. R., Levan, A. J., et al. 2019, ApJ, 883, 48
Lantz, B., Aldering, G., Antilogus, P., et al. 2004, SPIE, 5249, 146
Leja, J., van Dokkum, P. G., Momcheva, I., et al. 2013, ApJL, 778, L24
Levan, A. J., Gompertz, B. P., Salafia, O. S., et al. 2024, Natur, 626, 737
Levan, A. J., Lyman, J. D., Tanvir, N. R., et al. 2017, ApJL, 848, L28
Li, L.-X., & Paczyński, B. 1998, ApJL, 507, L59
Licandro, J., Tonry, J., Alarcon, M. R., Serra-Ricart, M., & Denneau, L. 2023, arXiv:2302.07954
Lipunov, V. M., Gorbovskoy, E., Kornilov, V. G., et al. 2017, ApJL, 850, L1
Magnier, E. A., Chambers, K. C., Flewelling, H. A., et al. 2020a, ApJS, 251, 3
Magnier, E. A., Schlafly, E. F., Finkbeiner, D. P., et al. 2020b, ApJS, 251, 6
Magnier, E. A., Sweeney, W. E., Chambers, K. C., et al. 2020c, ApJS, 251, 5
McCully, C., Hiramatsu, D., Howell, D. A., et al. 2017, ApJL, 848, L32
Metzger, B. D. 2017, LRR, 20, 3
Metzger, B. D., Hui, L., & Cantiello, M. 2024, ApJL, 971, L34
Metzger, B. D., Martínez-Pinedo, G., Darbha, S., et al. 2010, MNRAS, 406, 2650
Metzger, B. D., & Piro, A. L. 2014, MNRAS, 439, 3916
Miao, H.-Y. 2022, Thesis, National Central University https://hdl.handle.net/11296/98q6x4
Müller-Bravo, T., & Galbany, L. 2022, JOSS, 7, 4508
Nicholl, M. 2018, RNAAS, 2, 230
Nicholl, M., & Andreoni, I. 2025, RSPTA, 383, 20240126
Nicholl, M., Berger, E., Kasen, D., et al. 2017, ApJL, 848, L18
Nicholl, M., Margalit, B., Schmidt, P., et al. 2021, MNRAS, 505, 3016
Nicholl, M., Young, D. R., Aamer, A., et al. 2025, GCN, 41439, 1
Nugent, A. E., Fong, W., Dong, Y., et al. 2020, ApJ, 904, 52
O'Connor, B., Troja, E., Dichiara, S., et al. 2022, MNRAS, 515, 4890
Oke, J. B., & Gunn, J. E. 1983, ApJ, 266, 713
Pastorello, A., Kasliwal, M. M., Crockett, R. M., et al. 2008, MNRAS, 389, 955
Pian, E., D'Avanzo, P., Benetti, S., et al. 2017, Natur, 551, 67
Piro, A. L., & Kollmeier, J. A. 2018, ApJ, 855, 103
Piro, A. L., Muhleisen, M., Arcavi, I., et al. 2017, ApJ, 846, 94
Planck Collaboration, Aghanim, N., Akrami, Y., et al. 2020, A&A, 641, A6
Rastinejad, J. C., Fong, W., Kilpatrick, C. D., Nicholl, M., & Metzger, B. D. 2025, ApJ, 979, 190
Rastinejad, J. C., Gompertz, B. P., Levan, A. J., et al. 2022, Natur, 612, 223
Richmond, M. W., Treffers, R. R., Filippenko, A. V., et al. 1994, AJ, 107, 1022
Rosswog, S., Sollerman, J., Feindt, U., et al. 2018, A&A, 615, A132
Schlafly, E. F., & Finkbeiner, D. P. 2011, ApJ, 737, 103
Schlegel, D., Dey, A., Herrera, D., et al. 2021, AAS Meeting, 237, 235.03
Schulze, S., Yaron, O., Sollerman, J., et al. 2021, ApJS, 255, 29
Shappee, B. J., Simon, J. D., Drout, M. R., et al. 2017, Sci, 358, 1574
Shingles, L., Smith, K. W., Young, D. R., et al. 2021, TNSAN, 7, 1
Smartt, S. J., Chen, T. W., Jerkstrand, A., et al. 2017, Natur, 551, 75
Smartt, S. J., Gillanders, J. H., Huber, M. E., et al. 2025, GCN, 41493, 1
Smartt, S. J., Nicholl, M., Srivastav, S., et al. 2024, MNRAS, 528, 2299
Smith, K. W., Smartt, S. J., Young, D. R., et al. 2020, PASP, 132, 085002
Soares-Santos, M., Holz, D. E., Annis, J., et al. 2017, ApJL, 848, L16
Speagle, J. S. 2020, MNRAS, 493, 3132
Srivastav, S., Smith, K. W., Smartt, S. J., et al. 2025, GCN, 41451, 1
Stein, R. 2025, TNSTR, 2025–3264, 1
Stein, R., Ahumada, T., Kasliwal, M., et al. 2025, GCN, 41414, 1
Stevance, H. F., Eldridge, J. J., Stanway, E. R., et al. 2023, NatAs, 7, 444
Stevance, H. F., Smith, K. W., Smartt, S. J., et al. 2025, ApJ, 990, 201
Tanaka, M., & Hotokezaka, K. 2013, ApJ, 775, 113
Tanvir, N. R., Levan, A. J., Fruchter, A. S., et al. 2013, Natur, 500, 547
Tanvir, N. R., Levan, A. J., González-Fernández, C., et al. 2017, ApJL, 848, L27
Tartaglia, L., Fraser, M., Sand, D. J., et al. 2017, ApJL, 836, L12
The LIGO Scientific Collaborationthe Virgo Collaborationthe KAGRA Collaboration 2025a, GCN, 41437, 1

The LIGO Scientific Collaborationthe Virgo Collaborationthe KAGRA Collaboration 2025b, arXiv:2508.18082
The LIGO Scientific Collaborationthe Virgo Collaborationthe KAGRA Collaboration 2025c, arXiv:2508.18080
Tonry, J. L., Denneau, L., Flewelling, H., et al. 2018a, ApJ, 867, 105
Tonry, J. L., Denneau, L., Heinze, A. N., et al. 2018b, PASP, 130, 064505
Tonry, J. L., Stubbs, C. W., Kilic, M., et al. 2012, ApJ, 745, 42
Troja, E., Fryer, C. L., O'Connor, B., et al. 2022, Natur, 612, 228
Troja, E., Piro, L., van Eerten, H., et al. 2017, Natur, 551, 71
Tucker, M. A., Shappee, B. J., Huber, M. E., et al. 2022, PASP, 134, 124502
Utsumi, Y., Tanaka, M., Tominaga, N., et al. 2017, PASJ, 69, 101
Valenti, S., David, Sand, J., et al. 2017, ApJL, 848, L24
Villar, V. A., Guillochon, J., Berger, E., et al. 2017, ApJL, 851, L21
Virtanen, P., Gommers, R., Oliphant, T. E., et al. 2020, NatMe, 17, 261
Wang, Q., Armstrong, P., Zenati, Y., et al. 2023, ApJL, 943, L15
Waters, C. Z., Magnier, E. A., Price, P. A., et al. 2020, ApJS, 251, 4
Weston, J. G., Smith, K. W., Smartt, S. J., Tonry, J. L., & Stevance, H. F. 2024, RASTI, 3, 385
Williams, R. D., Francis, G. P., Lawrence, A., et al. 2024, RASTI, 3, 362
Wright, D. E., Smartt, S. J., Smith, K. W., et al. 2015, MNRAS, 449, 451
Yang, Y.-H., Troja, E., O'Connor, B., et al. 2024, Natur, 626, 742
Yu, Y.-W., Zhang, B., & Gao, H. 2013, ApJL, 776, L40